ELSEVIER

Coordination Chemistry Reviews 224 (2002) 11–34

COORDINATION CHEMISTRY REVIEWS

www.elsevier.com/locate/ccr

Coordination compounds of 1,4-dihydroxybenzoquinone and its homologues. Structures and properties

Susumu Kitagawa [a,*], Satoshi Kawata [b]

[a] *Department of Synthetic Chemistry and Biological Chemistry, Graduate School of Engineering, Kyoto University, Yoshida, Sakyo-ku, Kyoto 606-8501, Japan*

[b] *Department of Chemistry, Faculty of Science, Shizuoka University, Oya, Shizuoka 422-8529, Japan*

Received 26 June 2000; received in revised form 26 February 2001; accepted 26 March 2001

Contents

Abstract

Metal complexes of 1,4-dihydroxy-benzoquinone and its homologues ($H_2C_6X_2O_4$) are reviewed, focusing on assembled structures based on their X-ray crystallographic structures reported so far. A wide variety of crystal structures based on mononuclear, binuclear, polynuclear complexes and extended structures of coordination polymers or hydrogen bond linked networks are listed in relation to the coordination modes such as the monodentate, bidentate, and bis-bidentate form of the

* Corresponding author.
E-mail address: kitagawa@sbchem.kyoto-u.ac.jp (S. Kitagawa).

PII: S0010-8545(01)00369-1

ligands. Their physico-chemical properties such as redox, UV–vis, EPR and magnetic properties are described. The ligand, $H_2C_6X_2O_4$, discussed here is one of the most useful multifunctional ligands, affording not only various self-assembled frameworks via coordination, hydrogen, and coulomb linkages, but also unique electronic structures, which are accompanied by charged and spin states. Their characteristics are mentioned in detail.

Keywords: Chloranilate; 1,4-Dihydroxybenzoquinone; Coordination polymer; Layer structure; Hydrogen bond network; Redox and magnetic properties

1. Introduction

Oxocarbon is one of the most useful multifunctional ligand families [1,2], and a large number of metal complexes have been synthesized to date. This article focuses on metal complexes of 1,4-dihydroxy-benzoquinone ($H_2C_6H_2O_4$) and its homologues since they can provide a variety of binding sites to metal cations and charged states. For instance, the dianionic form has five coordination modes shown in Scheme 1, which afford intriguing crystal structures and physico-chemical properties. The derivatives are obtained by replacing a hydrogen atom with a substituent, X, which are summarized as $H_2C_6X_2O_4$ in Table 1 [3–25]. With the aid of these coordination modes, both finite and extended molecular assemblies have been developed. In practice, the redox and/or magnetic properties have added a new dimension to the coordination chemistry, and therefore, this family is opening up a field of compound-based materials [26–70]. In addition, the crystal structures have afforded a variety of frameworks together with voids. The frameworks are listed as chains, ladders, grids, honeycomb, and so on (Fig. 1) while voids are classified in cavities, channels and space between layers, illustrating an alternative to inorganic zeolites and clays [71]. There are two types of the solid state structures: one is a supramolecular assembly of low-molecular weight modules of metal complexes of $H_2C_6X_2O_4$ while the other is an infinite extended structure constructed by coordination bonds, i.e. coordination polymers. The coordination polymers are prepared from a monomeric unit with bis (1) or tris (2) coordination of $C_6X_2O_4$. The bis form essentially provides a one-dimensional (1D) framework, and a two-dimensional (2D) one can be obtained when another linking ligand is used. On the other hand, the tris form affords 2D honeycomb lattices and three-dimensional (3D) structures (Fig. 1). For both monomer and coordination polymer motifs, hydrogen-bonds play an important role to construct extended arrays. Assemblies of 1D polymers organized through hydrogen bonding interactions between coordinated water molecules and oxygen atoms of the ligands have been reported [72–78]. Fig. 2 shows a conceptual scheme of hydrogen-bonding, together with the intercalation of guest molecules in the layer spacing. On the other hand, a tris-type building block, i.e. octahedral $M(C_6X_2O_4)_3$ module, are interlinked by their own chelating dianions to give a honeycomb-type sheet network. Interestingly, adjacent layers tend to be connected by hydrogen bonds of interstitial guest molecules such as water.

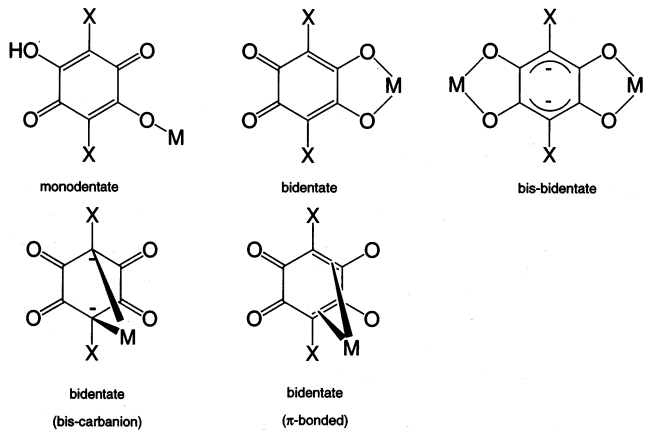

Scheme 1.

Table 1
Abbreviations of $H_2C_6X_2O_4$

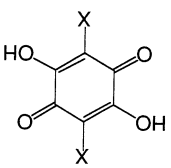

X	Abbreviation	Reference
H	H_2dhbq	[12,13]
F	H_2fa	[9]
Cl	H_2ca	[3–8,11,16]
Br	H_2ba	[25]
I	H_2ia	[24]
NO_2	H_2na	[6,7,10,17]
CN	H_2(CN_2dhbq)	[10]
OH	H_2(thbq)	[18,19]
CH_3	H_2(Me_2dhbq)	[15]
C_2H_5	H_2(Et_2dhbq)	[20]
C_6H_5	H_2(Ph_2dhbq)	[21]
iso-C_3H_7	H_2(Pr_2dhbq)	[23]

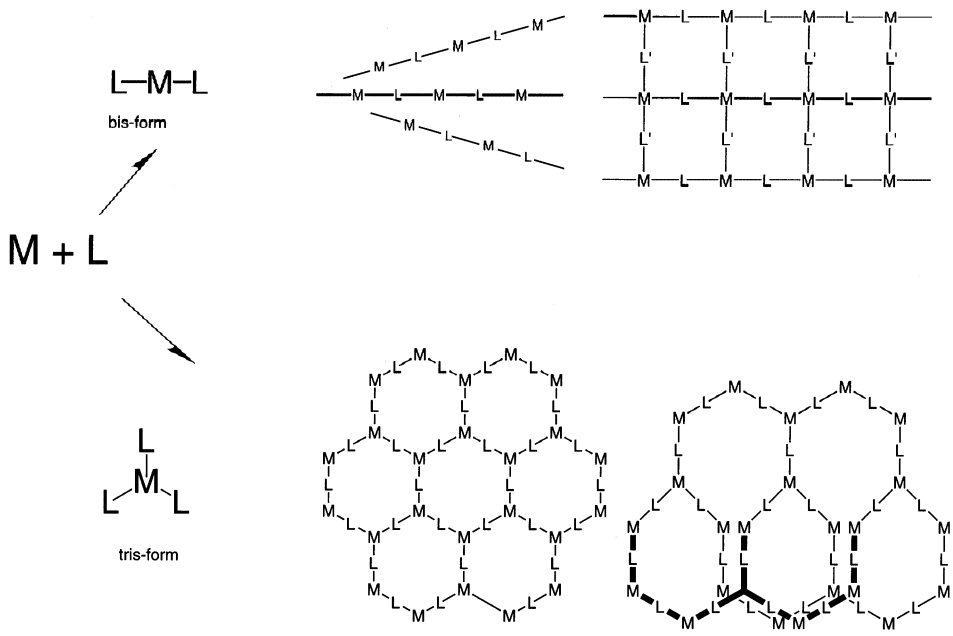

Fig. 1. Frameworks constructed from bis- and tris-coordination modules.

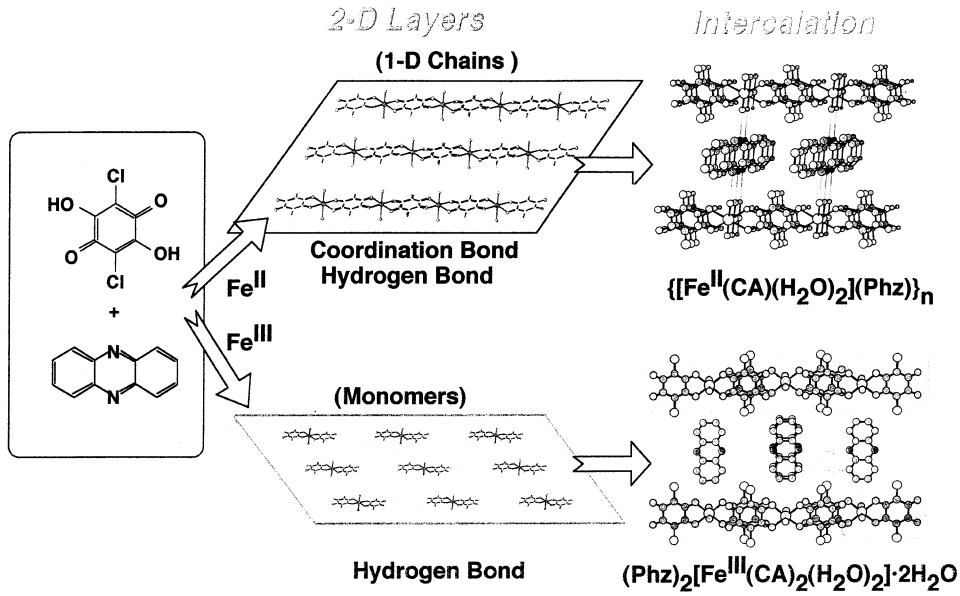

Fig. 2. Formations of sheet structures based on coordination bond and/or hydrogen-bonding frameworks, and intercalation of guest molecules.

This article begins with a survey of the structural coordination chemistry of 1,4-dihydroxy-benzoquinone and its homologues ($H_2C_6X_2O_4$), focusing on supramolecular assemblies and coordination polymers, and then, discusses physico-chemical properties in relation not only to basic coordination chemistry but also to material chemistry.

2. Structural classification of crystal structures

2.1. Lower nuclearity compounds

2.1.1. Mononuclear compounds

The monomeric compounds are usually obtained as mono-, bis-, and tris-forms of $C_6X_2O_4$ dianions, which

are listed in Table 2. They are all considered as candidates for a synthon of supramolecular assemblies because of the metal-free oxygen sites. Among the mononuclear complexes, the chloranilate dianion provides three coordination modes, which are associated with a linkage isomerism: (A) bis-carbanion, (B) *p*-quinone and (C) *o*-quinone chloranilate in transition metal complexes (Fig. 3 and Table 2). This characteristic coordination mode reflects the bonding nature of the metal ion, whose steric and electronic factors influence the interconversion of sp^2- and sp^3-hybridized C atoms in the first coordination sphere.

A mononuclear species $[MoO_2(ca)(Hca)]^-$ was obtained from $[Mo_2O_7]^{2-}$ or $[Mo_8O_{26}]^{4-}$ [79,80]. Because the complex is a monoanion, the chloranilate ligands are inequivalent and have an *o*-quinone-like structure: the mean C–O distance at uncoordinated sites in ca^{2-} is the normal benzoquinone distance for double bond localization in the carbonyl group (1.21 Å). In contrast, that in Hca^- is apparently longer (1.25 Å). On this basis, a broad peak at 3540 cm^{-1} in the IR spectrum indicates the presence of an exchangeable proton on one ligand site.

The bis-carbanion ligation (type A) through the C–Cl carbon atoms is found in $K_2[Pd(ca)Cl_2]\cdot nH_2O$ [81]. Some 16 $[Pd(ca)L_2]$ compounds were examined spectroscopically by changing L [82–85]. $[Pd(ca)\{P(\mu\text{-}C_7H_7)_3\}_2]$ exhibits a distorted square-planar P_2O_2 ligand field about the Pd(II) atom [86]. The coordinated chloranilate C–C and C–O bond lengths reveal a predominant *o*-quinone resonance form (type C), in contrast to the delocalized *p*-quinone structure (type B) characteristic of bridging chloranilate in transition metal complexes [87]. In the compound, $[Pd(ca)(CH_3CN)_2]$, chloranilate ligates Pd(II) through both C–Cl carbon atoms, with Pd–C bond lengths of 2.089(5) and 2.093(6) Å, indicating that the chloranilate has the bis-carbanion (type A) geometry (Fig. 4) [88].

2.1.2. Dinuclear compounds

There are two types of structural feature in the dinuclear compounds. One is the bridged type, $[M_2(L)_2(C_6X_2O_4)]^{n+}$ and the other is the terminal type, $[M_2(L)(C_6X_2O_4)_2]^{n+}$. Discrete dimeric compounds, $[M_2(L)_2(ca)]^{n+}$ have a centrosymmetric structure of the metal atoms bridged by ca^{2-} dianions in a bis-bidentate fashion. The structural features of the bridging dianion in the dimers can be divided into two types: (1) delocalized structure and (2) localized structure. In the former case, the dianions are essentially planar with delocalization of π-electrons, and the latter type has localized *p*-quinone structure (Scheme 2 and Table 2). The structure of iron(III) chloranilate, $[Fe_2(C_6Cl_2O_4)_3(H_2O)_4]4H_2O$, has been determined by single crystal X-ray diffraction, revealing a dinuclear structure with one bridging chloranilate, two *cis* water ligands and one chelating, 'terminal' chloranilate per iron(III) center [89].

On the other hand, reduced $C_6X_2O_4^{n-}$ anions also make dinuclear compounds. Cooperation of counter-ligand, tripodal phosphane $CH_3C(CH_2PPh_2)_3$, and cobalt ion affords a stable tetraanion L_4 shown in Scheme 2. Fig. 5 shows a dinuclear cobalt(III) dication $[Co_2(dhbq)(tdpme)_2](BF_4)_2\cdot CH_2Cl_2$[90]. The C–O distances (1.313(8) and 1.311(8) Å), longer than those of $dhbq^{2-}$, indicate the absence of a delocalized quinoid structure. The bridging ligand is best depicted as a tetraanionic type, [cat,cat], form. On the other hand, the trianion form [sq,cat] of L_3 is realized in an iron complex of a tetraazamacrocycle. Complexes $[Fe_2(dhbq)_2(CTH)_2]Y\cdot nH_2O$ ($Y = ClO_4^-$, PF_6^-) have a dinuclear structure of two iron(III) ions with one bridging dhbq [91].

2.1.3. Oligomeric compounds

A centrosymmetric tetranuclear complex, $[Rh_4(ca)_2(cod)_4]$, displays a novel coordination mode of each ca dianion in the *o*-quinone form, which interacts with three rhodium atoms via three σ-bonds through the oxygen atoms and two π-bonds through two adjacent double bonds (Fig. 6) [92]. The structure of $\{(n\text{-}C_4H_9)_4N\}_2[Mo_4O_{10}(dhbq)_2]$ consists of discrete tetra nuclear dianionic units $[Mo_4O_{10}(dhbq)_2]^{2-}$ (Fig. 7) [79,80,93]. The dhbq ligands function as bis-bidentate groups bridging two $[Mo_2O_5]^{2+}$ units. The Mo coordination sites in the complex consist of two sets of two distorted $[MoO_6]$ octahedra sharing a common face to give a cofacial bioctahedral geometry. The dhbq ligands coordinate formally as radical anions of L_3 type in Scheme 2, whose formulation is consistent with the C–O bond lengths which average 1.29(1) Å, intermediate between values of 1.22 Å found for benzoquinones and 1.38 Å for hydroquinones.

2.2. Hydrogen bond-linked layer compounds of discrete molecules

$[Cu_2(ca)_2(H_2O)_2(bpym)]$ shows a bpym-bridged dicopper unit with the terminally coordinated *o*-quinone form of chloranilate (Fig. 8) [94]. The chloranilate shows symmetrical coordination with two equal Cu–O distances (1.91 Å). The apically coordinated water molecules and the metal-free ca oxygen atoms are important for the hydrogen-bonded network; the two nearest neighbor hydrogen bonds (2.75 and 2.78 Å), forming a 2D layer with the interlayer distance of 7.6 Å. This is representative of supramolecular assemblies involving the dhbq family, where in principle, this type of hydrogen-bonded link is operative.

Table 2

Compound	Type	M–O distance (Å)	C–O distance (Å)	Reference
Mononuclear compounds				
$(C_{21}H_{38}N)_2[Be(ca)_2]$	*o*-quinone	1.639, 1.620	1.296, 1.291, 1.220, 1.222	[154]
$Na_2{\cdot}[UO_2(ca)_2]$	*o*-quinone	2.373	1.263, 1.234	[155]
$[(C_4H_9)_4N][MoO_2(ca)(Hca)]$	*o*-quinone	2.042, 2.202, 2.187, 2.031	1.311, 1.292, 1.276, 1.315, 1.241, 1.259, 1.225, 1.197	[79,80]
$[C_6H_{16}N]_3[In(ca)_3]{\cdot}2H_2O$	*o*-quinone	2.133	1.272, 1.233	[156]
$[FeCl(ca)(H_2O)_3]{\cdot}5H_2O$	*o*-quinone	2.007, 2.087	1.282, 1.284 1.227, 1.237	[157]
$[Cu(terpy)(ca)]2H_2O$	*o*-quinone	2.042, 2.054	1.268, 1.273, 1.228, 1.232	[137]
$[Cu(dhbq)(bpym)(H_2O)]{\cdot}5H_2O$	*o*-quinone	1.947, 1.928	1.287, 1.303, 1.251, 1.240	[158]
$[Cu(ca)(C_{14}H_{12}N_2O_4)(H_2O)]{\cdot}0.5CH_3CN$	*o*-quinone	1.938, 1.947	1.278, 1.273, 1.223, 1.235	[159]
$[Ni(dhbq)(Me_2bpy)_2]{\cdot}H_2O$	*o*-quinone	2.056, 2.043	1.279, 1.290, 1.240,1.240	[158]
$[Pd(ca)\{P(m\text{-}C_7H_7)_3\}_2]$	*o*-quinone	2.047, 2.054	1.284, 1.292, 1.230, 1.225	[86]
$[Pd(ca)\{P(n\text{-}C_4H_9)_3\}_2]$	*o*-quinone	2.045, 2.064	1.282, 1.291, 1.255, 1.196	[87]
$[Pd(ca)Cl_2]$	bis-carbanion	M–C (2.018, 2.069)	1.266, 1.268	[81]
$[Pd(ca)(CH_3CN)_2]$	bis-carbanion	2.092, 2.089	1.217, 1.213, 1.211, 1.210	[88]
Dinuclear compounds				
$[Ni_2(tren)_2(ca)](BPh_4)_2$	bis-bidentate (delocalized)	2.044, 2.129	1.265, 1.251	[135]
$[Cu_2(Me_5dien)_2(ca)](BPh_4)_2$	bis-bidentate (delocalized)	2.196, 1.955	1.243, 1.257	[135]
$[Cu_2(terpy)_2(ca)](PF_6)_2$	bis-bidentate (localized)	2.267, 1.943	1.244, 1.266	[136]
$[Cu_2(bipy)_2(ca)(CH_3OH)_2](PF_6)_2$	bis-bidentate (delocalized)	1.940, 2.022	1.262, 1.261	[138]
$[Cu_2(Me_3\text{-}tacn)_2(ca)](ClO_4)_2$	bis-bidentate (delocalized)	1.999, 1.968	1.251, 1.268	[140]
$[Cu_2(tmen)_2(ia)(CH_3OH)_2](ClO_4)_2$	bis-bidentate (localized)	1.956, 1.952	1.266, 1.263	[137]
$[(n\text{-}C_4H_9)_4N]_2[Mo_2O_4Cl_4(ca)]{\cdot}0.5CH_3CN$	bis-bidentate (delocalized)	2.202, 2.042, 2.187, 2.031	1.311, 1.292, 1.315, 1.276, 1.241, 1.259, 1.225, 1.197	[79,119]
$[Rh_2(ca)(cod)_2]$	bis-bidentate (delocalized)	2.089, 2.100	1.257, 1.283	[92]
$[Rh_2(ca)Me_2I_2(CO)_2(PPh_3)_2]$	bis-bidentate (delocalized)	2.090, 2.190	1.269, 1.266	[160]
$[Co_2(dhbq)(tdpme)_2]^{2+}$	bis-bidentate (localized)	1.898, 1.884	1.313, 1.312	[90]
$[Co_2(ca)(tdpme)_2]^{2+}$	bis-bidentate (localized)	1.881, 1.876	1.321, 1.311	[90]
$[Co_2(ba)(tdpme)_2]^{2+}$	bis-bidentate (localized)	1.864, 1.863	1.327, 1.312	[90]
$[Pt_2(dhbq)(C_6F_5)_4]^2$	bis-bidentate (delocalized)	2.107, 2.095	1.273, 1.274	[161]
$[Mn_2(tpa)_2(ca)](ClO_4)_2{\cdot}3H_2O$	bis-bidentate (delocalized)	2.213, 2.154	1.252, 1.251	[146]
$[Mn_2(tpa)_2(ca)]{\cdot}(ClO_4)_2{\cdot}2CH_3CN$	bis-bidentate (delocalized)	2.149, 2.242	1.255, 1.256	[146]
$[Fe_2(ca)_3(H_2O)_4]$	bis-bidentate (delocalized), *o*-quinone	1.978, 1.995	1.254, 1.266 1.287, 1.291, 1.223, 1.225	[89]
$[Pd_2(ca)_2Cl_2]$	bis-carbanion	M–C (2.015, 2.044)	1.292, 1.291, 1.289, 1.284	[81]
Oligomeric compounds				
$[Rh_4(ca)_2(cod)_4]$	*o*-quinone	2.105, 2.079	1.276, 1.282, 1.218, 1.215	[92]
$[Mo_4O_{10}(dhbq)_2]^{2-}$	bis-bidentate (delocalized), radicals on them	2.231, 2.003	1.299, 1.280	[79,80,93]
Hydrogen bond-linked layer compounds of discrete molecules				
$[Cu_2(ca)_2(H_2O)_2(bpym)]$	*o*-quinone	1.907, 1.907	1.27, 1.26, 1.24, 1.23	[94]
Chain structures: straight and zigzag chains				
$\{[Cu(ca)(H_2O)](ohphz)\}_n$	bis-bidentate (delocalized)	1.960	1.273	[74]
$[Cu(dcmb)(ca)]_n$	bis-bidentate (localized)	2.238, 1.999	1.237, 1.269	[95]
$[Mn(bpy)(ca)]_n$	bis-bidentate (delocalized)	2.180, 2.183	1.257, 1.250	[96]
$[Mn(terpy)(ca)(H_2O)]_n$	bis-bidentate (delocalized)	2.293, 2.188	1.256, 1.250	[105]
$[Ag_2(ca)]_n$	delocalized	2.468, 2.461, 2.442, 2.375	1.247, 1.239	[97]
$[Na_2(ca)(H_2O)_3]_n$	delocalized	2.358, 2.399	1.246, 1.252, 1.255, 1.259	[109]
$[Na_2(phen)(ca)]_n(H_2O)_2$	delocalized	2.436, 2.364	1.231, 1.241	[109,162]
$\{[Co(ca)(bpym)](H_2O)_2\}_n$	bidentate(*o*-quinone)	2.065	1.278, 1.232	[163]
Sheet structures of 1D + 1D				
$[Cu(ca)(CH_3OH)_2]_n$	bis-bidentate (delocalized)	1.963, 2.005	1.262, 1.258	[98]
$[Cu(ca)(H_2O)_2]_n$	bis-bidentate (localized)	1.995, 1.884	1.305, 1.283	[74]
$\{[Sr(Ph_2dhbq)_2O_4)]{\cdot}4H_2O\}_n$	bis-bidentate (delocalized)	2.617, 2.532	1.268	[21]
$\{[Ba(Ph_2dhbq)_2O_4)]{\cdot}4H_2O\}_n$	bis-bidentate (delocalized)	2.766, 2.667	1.238, 1.271	[21,22]
Hydrogen bond-supported 3D systems				
$[Zn(na)(H_2O)_2]_n$	bis-bidentate (delocalized)	2.133, 2.075	1.236, 1.244	[99]
$[Sr(na)(H_2O)_2]_n$	bis-bidentate (delocalized)	2.738, 2.575	1.233, 1.237	[100]

Table 2 (*Continued*)

Compound	Type	M–O distance (Å)	C–O distance (Å)	Reference
$[Ca(na)(H_2O)_2]_n$	bis-bidentate (delocalized)	2.579, 2.435	1.245, 1.239	[100]
$[Ba(Et_2dhbq)(H_2O)_3]_n$	bis-bidentate (delocalized)	2.912, 2.730, 2.745, 2.741	1.319, 1.243, 1.262, 1.258	[20]
$[Ca(Et_2dhbq)(H_2O)_3]_n$	bis-bidentate (delocalized)	2.547, 2.372, 2.426, 2.390	1.304, 1.267, 1.255, 1.272	[20,101]
$[Sr(Et_2dhbq)(H_2O)_3]_n$	bis-bidentate (delocalized)	2.697, 2.556, 2.583, 2.551	1.302, 1.261, 1.239, 1.261	[20]
Honeycomb lattices				
$\{Na_2(H_2O)_{24}[Mn_2(dhbq)_3]\}_n$	bis-bidentate (delocalized)	2.168	1.276	[102]
$\{Na_2(H_2O)_{24}[Cd_2(dhbq)_3]\}_n$	bis-bidentate (delocalized)	2.264	1.272	[102]
$\{[Ce_2(dhbq)_3]\cdot 24H_2O\}_n$	bis-bidentate (delocalized)	2.541, 2.482	1.270, 1.262	[103]
$\{[Y_2(ba)_3(H_2O)_6]\cdot 6H_2O\}_n$	bis-bidentate (delocalized)	2.500, 2.400, 2.399, 2.389, 2.348, 2.342	1.248, 1.241, 1.224, 1.245, 1.240, 1.237	[104]
$\{[Y_2(ca)_3(H_2O)_6]\cdot 6.6H_2O\}_n$	bis-bidentate (delocalized)	2.405, 2.393	1.251, 1.252	[104]
$\{[Mn(ca)(bpym)_{0.5}(H_2O)]\cdot H_2O\cdot EtOH\}_n$	bis-bidentate (delocalized)	2.222, 2.304	1.246, 1.255	[105]
Rectangular lattice				
$[Cu(ca)(pyz)]_n$	bis-bidentate (delocalized)	2.290, 1.955	1.233, 1.281	[98]
Other layers				
$[Ca(Pr_2dhbqH)]\cdot 2/3H_2O$	*o*-quinone	2.422, 2.345, 2.273	1.257, 1.244, 1.284, 1.342	[23]
$\{[Ba(ca)(H_2O)_2](H_2O)\}_n$	*o*-quinone	2.787, 2.766	1.269, 1.250	[106]
$\{[Ba(ba)(H_2O)_2](H_2O)\}_n$	*o*-quinone	2.792, 2.799	1.279, 1.248	[106]
$[Sr(ca)(H_2O)_4]_n$	*o*-quinone	2.551, 2.553	1.263, 1.245	[107]
$[Sr(ba)(H_2O)_4]_n$	*o*-quinone	2.571, 2.573	1.256, 1.249	[107]
$[Ca(ca)(H_2O)_4]_n$	*o*-quinone	2.441, 2.409	1.257, 1.252	[107]
$[Ca(ba)(H_2O)_4]_n$	*o*-quinone	2.438, 2.417	1.271, 1.253	[107]
$[Ba(ca)(H_2O)_4]_n$	*o*-quinone	2.553, 2.551	1.245, 1.263	[107]
3D structures				
$\{[Pr_2(ca)_3(C_2H_5OH)_6](C_2H_5OH)_2\}_n$	bis-bidentate (delocalized)	2.50, 2.499	1.252, 1.249	[110]
$[K_2(dhbq)]_n$	delocalized	2.819, 2.692	1.263, 1.264	[12]
$[K_2(na)]_n$	delocalized	3.021, 2.931, 2.777	1.219	[111]
$[Na_2(na)]_n$	delocalized	2.424, 2.404	1.230, 1.227	[111]
$[Na(ca)(H_2O)]_n$	delocalized	2.300	1.250, 1.245, 1.248, 1.260	[108]
Host systems based on 1D polymers				
$\{[Cu(ca)(H_2O)_2](phz)\}_n$	bis-bidentate (localized)	2.228, 2.073	1.241, 1.275	[74]
$\{[Co(ca)(H_2O)_2](phz)\}_n$	bis-bidentate (localized)	2.109, 2.083	1.248, 1.264	[73]
$\{[Mn(ca)(H_2O)_2](phz)\}_n$	bis-bidentate (localized)	2.183, 2.196	1.263, 1.252	[73]
$\{[Fe(ca)(H_2O)_2](phz)\}_n$	bis-bidentate (localized)	2.133, 2.148	1.274, 1.249	[73]
$\{[Cu(ca)(H_2O)_2](dmpyz)\}$ (a)	bis-bidentate (localized)	2.225, 2.057	1.245, 1.270	[74]
$\{[Cu(ca)(H_2O)_2](dmpyz)\}$ (b)	bis-bidentate (localized)	2.323, 1.982	1.250, 1.267	[74]
$\{[Cu(ca)(H_2O)_2](H_2O)\}_n$	bis-bidentate (localized)	1.966, 2.265	1.279, 1.241	[72,164]
$\{[Fe(ca)(H_2O)_2](H_2O)\}_n$	bis-bidentate (delocalized)	2.123, 2.152	1.256, 1.258	[73,89]
$\{[Co(ca)(H_2O)_2](H_2O)\}_n$	bis-bidentate (delocalized)	2.118, 2.098	1.257, 1.258	[73]
$\{[Mn(ca)(H_2O)_2](H_2O)\}_n$	bis-bidentate (delocalized)	2.193, 2.191	1.262, 1.252	[73]
Host systems based on monomer compounds				
$\{[Fe(Cp)_2][Fe(ca)_2(H_2O)_2]\}_n$	*o*-quinone	1.983	1.26, 1.22	[94]
$\{(Hphz)[Fe(ca)_2(H_2O)_2]\}_n$	*o*-quinone	1.996	1.281, 1.227	[77]
$\{(Hpy)[Fe(ca)_2(H_2O)_2]\}_n$	*o*-quinone	1.961, 2.021, 1.991, 1.982	1.284, 1.273, 1.285, 1.285, 1.230, 1.236, 1.238, 1.242	[76]
$\{(H_2bpy)_{0.5}[Fe(ca)_2(H_2O)_2]\}_n$	*o*-quinone	1.975, 2.005, 2.010, 1.992	1.293, 1.284, 1.295, 1.288, 1.224, 1.225, 1.224, 1.232	[76]
$\{(4\text{-}pyOH_2)_{0.5}[Cu(ca)_2(H_2O)_2]\}_n$	*o*-quinone	1.962, 1.937	1.274, 1.276, 1.232, 1.234	[75]
$\{(3\text{-}pyOH_2)_{0.5}[Cu(ca)_2(H_2O)_2]\}_n$	*o*-quinone	1.946, 1.944	1.275, 1.271, 1.229, 1.244	[75]
$\{(3\text{-}pyOH_2)_{0.5}[Co(ca)_2(H_2O)_2]\}_n$	*o*-quinone	2.069, 2.125, 2.065, 2.114	1.265, 1.278, 1.235, 1.250, 1.262, 1.281, 1.232, 1.249	[75]

2.3. Coordination polymers

2.3.1. Chain structures: straight and zigzag chains

$\{[Cu(ca)(H_2O)](ohphz)\}_n$ has an infinite chain formed by Cu^{2+} ions and the bis-chelating chloranilate anions (Fig. 9) [74]. The oxygen atoms of the dianion are equally bound to Cu^{2+}; all the Cu–O distances are 1.96 Å. The bond lengths in the dianion (C–C distances are 1.39 and 1.56 Å) are typical of completely delocalized π-electrons (*p*-quinone resonance form, L_2) as illus-

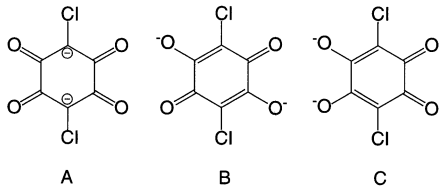

Fig. 3. (A) Bis-carbanion, (B) *p*-quinone (C) *o*-quinone chloranilate forms in ca^{2-}.

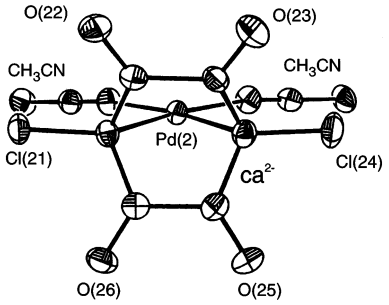

Fig. 4. ORTEP view of $[Pd(ca)(CH_3CN)_2]$ (original Fig. 1 from Ref. [88]).

trated in Scheme 2. Interestingly, non-planar ohphz molecules sit between the chains and are anchored by the N(1)···O(1) and N(1′)···O(1′) hydrogen bonding in a manner parallel to the chain direction, resulting in no hydrogen bonding links between chains. $[Cu(dcmb)(ca)]_n$ has an infinite zigzag chain formed by Cu(ca) module (Fig. 10) [95]. The oxygen atoms of the dianion are not equally bound to Cu^{2+}; the Cu–O distances are 1.999(1) and 2.238(1) Å. The effect of the asymmetrical coordination is also found in the different C–O distances in the dianion (1.270(2) and 1.237(2) Å), indicating that the dianion has a *p*-quinone form. The intermolecular Cu···Cu separation within a chain is 7.980(3) Å.

The crystal of $[Mn(bpy)(ca)]_n$ is built from infinite chains of ca^{2-}-bridged manganese(II) affording a zigzag structure, with the bipyridine ligands being stacked between the chains (Fig. 11) [96]. The manganese atoms are coordinated in a distorted octahedral arrangement by two nitrogen atoms of bpy and four oxygen atoms of the bridging dianion with *p*-quinone

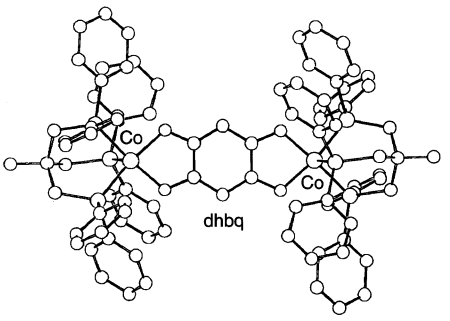

Fig. 5. Perspective view of the dianion of $[Co_2(dhbq)(tripod)_2]^{2-}$ (original Fig. 4 from Ref. [90]).

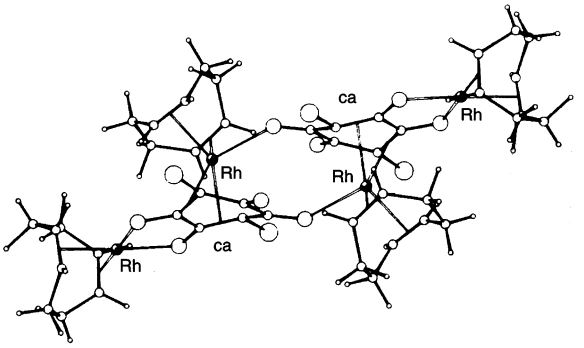

Fig. 6. View of $[Rh_4(ca)_2(cod)_4]$ (original Fig. 2 from Ref. [92]).

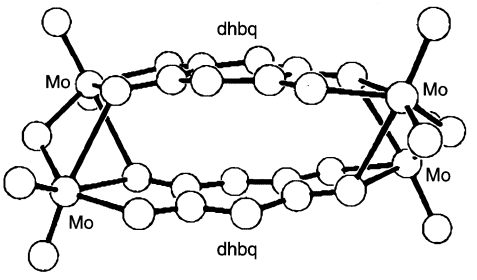

Fig. 7. ORTEP view of $[Mo_2O_4Cl_4(ca)]^{2-}$ (original Fig. 3 from Ref. [119]).

form. The distance between adjacent Mn(II) atoms inside a chain is 8.142(1) Å, which is larger than that of $[Cu(dcmb)(ca)]_n$ [95]. For an oxygen atom of ca, both

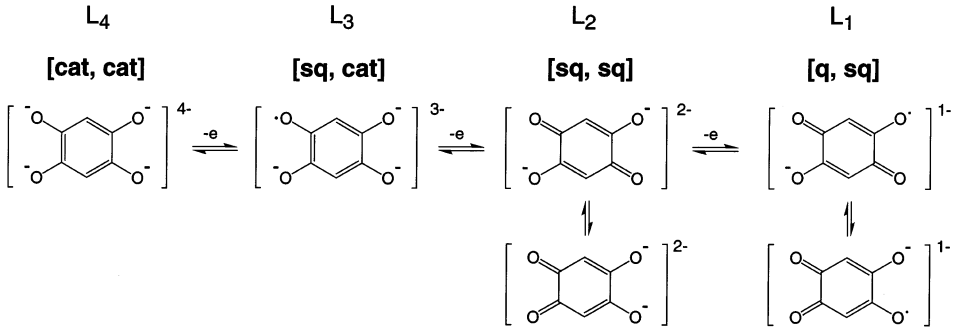

Scheme 2.

bridging μ_2 and chelating types occur simultaneously in $[Ag_2(ca)]_n$, resulting in an infinite chain (Fig. 12) [97]. Crossing chains are connected by Ag–O and Ag–Cl contacts. The Ag–O distances are 2.37–2.47 Å and the Ag–Cl distance is 2.81 Å.

2.3.2. Sheet structures based on 1D chains

Interestingly, there are several infinite chains, which are linked together by hydrogen bonds to form 2D sheets. Oxygen atoms of dhbq and its derivatives play an important role in the hydrogen bonding network, as do coordinated hydrogen donor ligands such as water and methanol. A single crystal of $[Cu(ca)(CH_3OH)_2]_n$ affords a 2D layer in which the straight 1D $[Cu(ca)(CH_3OH)_2]_n$ chains are interlinked by two hydrogen bonds (O–O distance: 2.845(3) Å) between apically coordinated MeOH and the oxygen atom of the dianion in the nearest neighbor chain (Fig. 13) [98]. A 2D layer is also found for $[Cu(ca)(H_2O)_2]_n$ in which the straight 1D chains are interlinked by hydrogen bonds

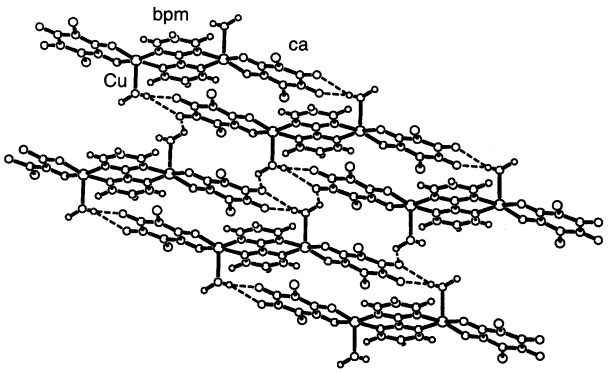

Fig. 8. Crystal structure of $[Cu_2(ca)(H_2O)_2(bpym)]$; view onto the *ab* plane. The dashed lines denote the hydrogen bonds (original Fig. 6 from Ref. [94]).

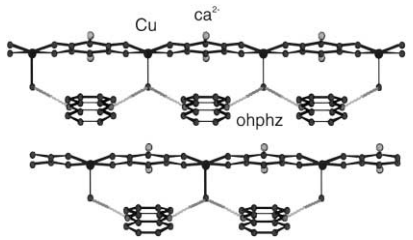

Fig. 9. The relationship between the chain and ohphz molecules in $\{[Cu(ca)H_2O)](ohphz)_n$ (original Fig. 5b from Ref. [74]).

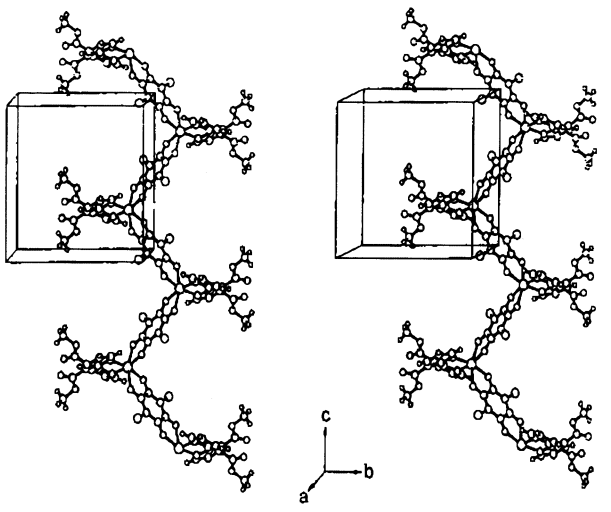

Fig. 10. Stereo view of the zigzag chain along the *c*-axis for [Cu(dcmb)(ca)]$_n$ (original Fig. 3 from Ref. [95]).

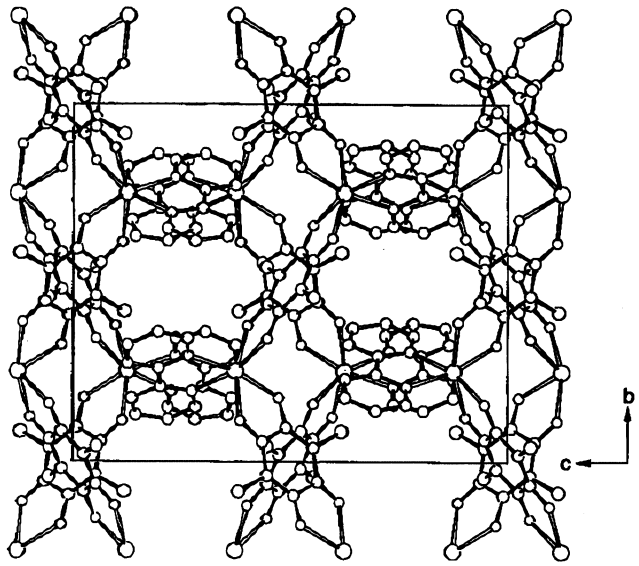

Fig. 11. [100] projection of the $[Mn(bpy)(ca)]_n$ chain (original Fig. 2 from Ref. [96]).

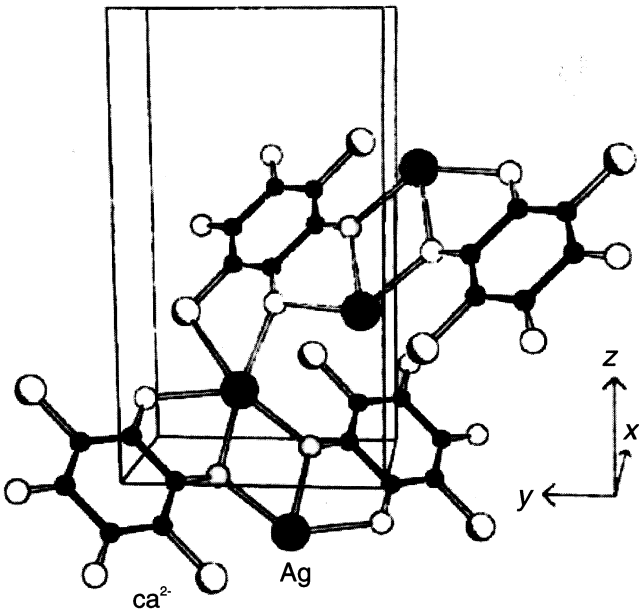

Fig. 12. SCHAKAL drawing of the chain for $[Ag_2(ca)]_n$ (original figure from Ref. [97]).

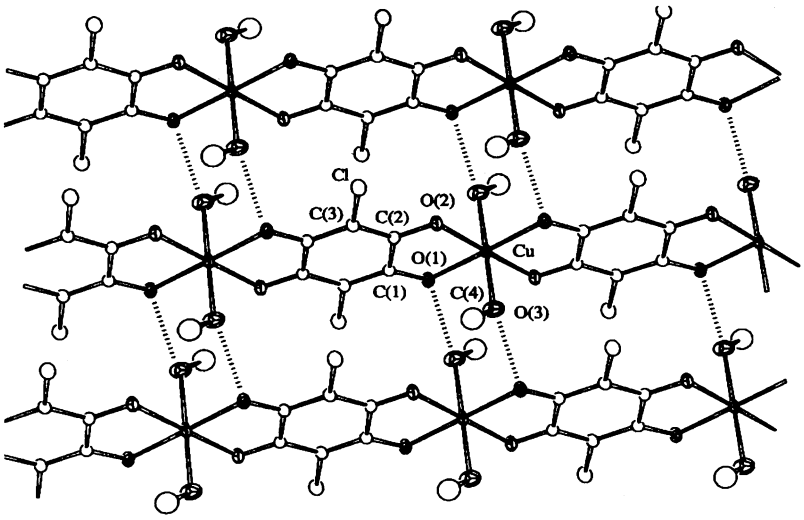

Fig. 13. Crystal structure of $[Cu(ca)(CH_3OH)_2]_n$ onto the *ac* plane (original Fig. 2 from Ref. [98]). Dotted lines show hydrogen bond link between coordinated water and chloranilate.

between the apically coordinated water molecules and the oxygen atoms of the dianions in the nearest neighbor chain (Fig. 14) [74]. The geometry around the copper atom is a distorted elongated octahedron. The interlayer distance is 8.45 Å. An infinite corrugated chain is found in $\{[M(Ph_2dhbq)_2O_4]\}\cdot 4H_2O\}_n$ ($M = Sr^{2+}$, Ba^{2+}) (Fig. 15) [21,22]. The coordination of oxygen atoms for $dhbq^{2-}$ is unsymmetrical both for Sr^{2+} and Ba^{2+}; the distances of M–O are (2.47 and 3.11 Å) and (2.680(3) and 2.769(3) Å), respectively. In both cases, the adjacent chains are interlinked by asymmetric hydrogen bonds thus forming layers.

When a functional group with hydrogen bonding capability is substituted in dhbq, additional hydrogen bonds occur in the crystal structure. $[Zn(na)(H_2O)_2]_n$ [99] has infinite corrugated chains of six coordinate distorted-octahedral zinc motifs with the two water molecules in *cis*-position (Fig. 16). These chains are interlinked by hydrogen bonds between H_2O and NO_2 groups. The NO_2 groups are twisted against the ring plane. The dianions are asymmetrically coordinated to the Zn atom, the distances of Zn–O being 2.075(2) and 2.133(3) Å, whereas the C–C distances are typical of completely delocalized π-electrons. $[M(na)(H_2O)_4]_n$ ($M = Ca^{2+}$, Sr^{2+}) [100] shows corrugated chains consisting of $M(na)(H_2O)_4$ motifs. For both compounds the adjacent chains are interlinked by hydrogen bonds. The bond lengths in the dianion are also typical of completely delocalized π-electrons. $[M(Et_2dhbq)(H_2O)_3]_n$ ($M = Ca^{2+}$, Sr^{2+}, and Ba^{2+}) [20,101] has infinite corrugated chains formed by M^{2+} and the bis-chelating anions. The structure of the dianion is similar in all the three compounds. There is a very slight tendency toward a system of alternating double bonds. Adjacent chains are interlinked by hydrogen bonds which involve oxygen atoms of the dianions and coordinated water hydrogen atoms as proton acceptors and donors, respectively.

2.3.3. Honeycomb lattices of tris-coordinate module

The infinite layers of complete coordination frameworks are obtained by transition metal ions ($M = Mn^{2+}$ and Cd^{2+}) in $\{Na_2(H_2O)_{24}[M_2(dhbq)_3]\}_n$ [102]. The octahedral $M(dhbq)_3$ modules are interlinked by their own chelating dianions to give a honeycomb-type sheet network. Adjacent layers are connected by hydrogen bonds of interstitial water molecules. The stacking sequence of these layers (···AAA···) leads to channels (Fig. 17), with hydrated Na^+ ions, which are coordinated in a distorted octahedral fashion with neighboring octahedra sharing common faces. The dianions in both compounds are almost planar with C–O bond (1.27 Å) and the two C–C bond (1.38 and 1.52 Å), distances characteristic of resonance stabilization. $\{[Ce_2(dhbq)_3]\cdot 24H_2O\}$ has infinite layers formed by Ce^{3+} and the bis-chelating anions, where Ce^{3+} is nine coordinate with three mutually *cis* water molecules and

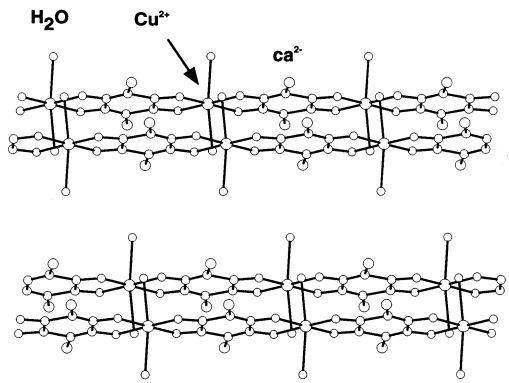

Fig. 14. Crystal structure of $[Cu(ca)(H_2O)_2]_n$ (original Fig. S1 from Ref. [74]).

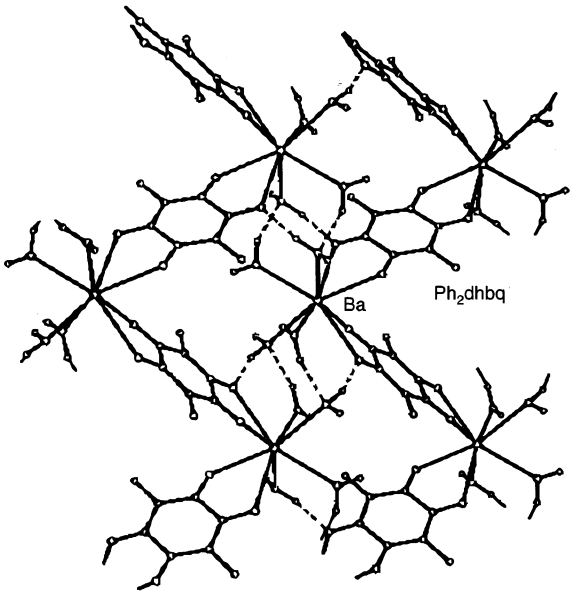

Fig. 15. Crystal structure of $\{[Ba(Ph_2dhbq)\cdot 4H_2O\}_n$. Connection of adjacent chains by asymmetric hydrogen bond (dashed lines). Phenyl groups on Ph_2dhbq dianions are omitted for clarity (original Fig. 2 from Ref. [22]).

six oxygen atoms of the dianions [78,103]. Each Ce^{3+} is interlinked by their own chelating dianions to give a honeycomb-type sheet network. It contains gas hydrate-like pentagonal dodecahedral $Ce_2(H_2O)_{18}$ cages which link together hexagonal grid sheets to form a 3D network (Fig. 18). A nine coordinate Y^{3+} module with a tricapped trigonal prism affords two isostructural compounds, $\{[Y_2(ba)_3(H_2O)_6]\cdot 6H_2O\}$ and $\{[Y_2(ca)_3(H_2O)_6]\cdot 6.6H_2O\}$ [104]. The connection of Y^{3+} with the dianions leads to infinite corrugated layers, which are interlinked by hydrogen bonds. The Y^{3+} cation is nine coordinate with three water molecules and six oxygen atoms of the dianions. The layer stacking yields cage-like cavities in which water molecules are accommodated. Hydrogen bonds interlink adjacent layers. Further hydrogen bonds involve the entrapped water molecules.

$\{[Mn(CA)(bpym)_{0.5}(H_2O)](H_2O)(C_2H_5OH)\}_n$ has a different type of honeycomb layer structure, where each hexagon consists of six Mn(II) ions, four ca^{2-} and two bipym ligands. Mn(II) ions in both the compounds are unusually hepta-coordinated [105].

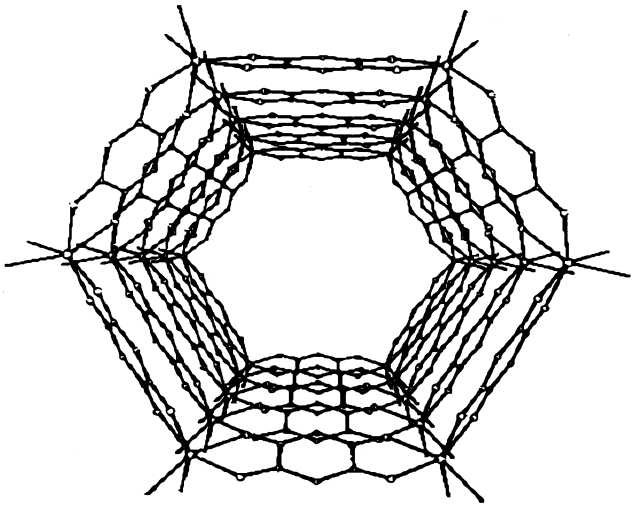

Fig. 17. Channel structure of $\{Na_2(H_2O)_{24}[Mn_2(dhbq)_3]\}_n$. The layers are stacked identically above each other, thus forming channels parallel to *c*-axis (original Fig. 2 from Ref. [102]).

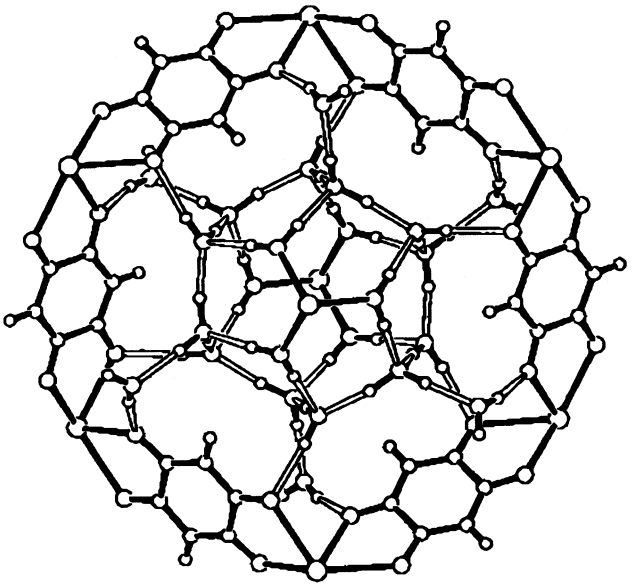

Fig. 18. Representation of a $Ce_2(H_2O)_{18}$ unit of one diamond-related framework passing through a $Ce_6(dhbq)_6$ ring of the other framework and the hydrogen-bonded links between the two in $\{[Ce_2(dhbq)_3]\cdot 24H_2O\}_n$ (original Fig. 2 from Ref. [103]).

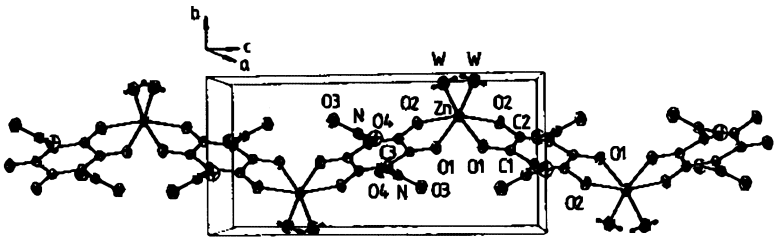

Fig. 16. Crystal structure of $[Zn(na)(H_2O)_2]_n$ (original Fig. 2 from Ref. [99]).

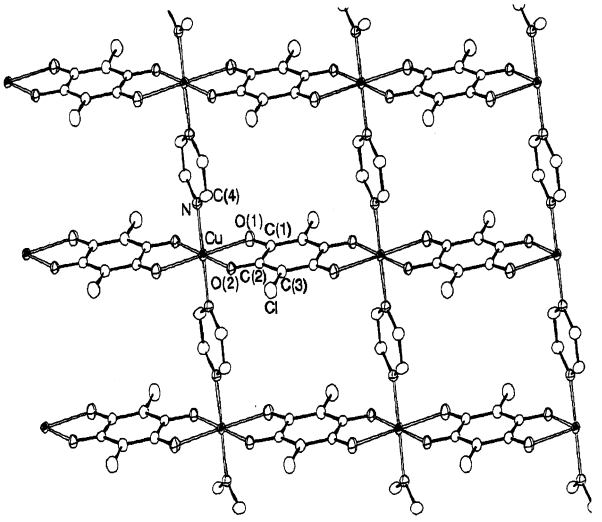

Fig. 19. Crystal structure of $[Cu(ca)(pyz)]_n$: view onto the bc plane (original Fig. 1 from Ref. [98]).

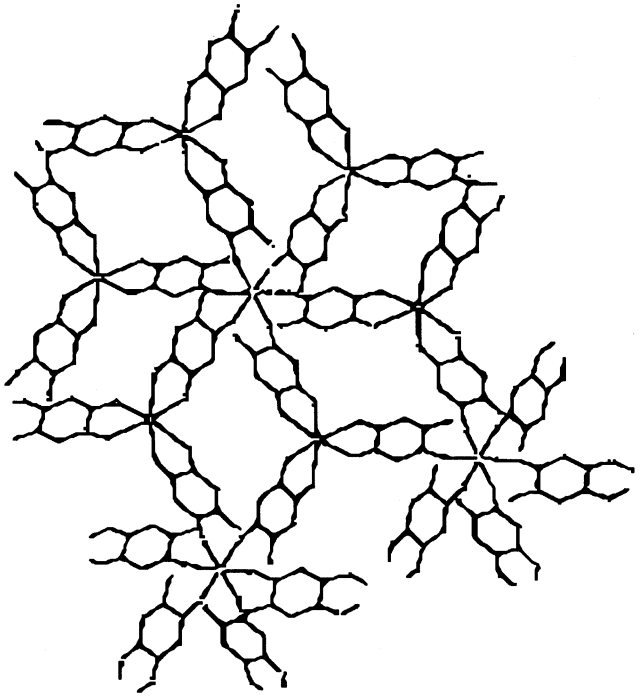

Fig. 20. Layer structure of $[Ca(Pr_2dhbq)O_4H)]\cdot 2/3H_2O$ (original Fig. 2 from Ref. [23]).

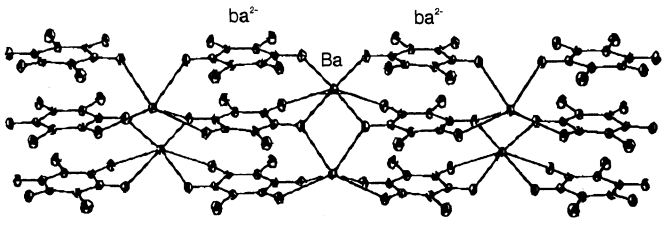

Fig. 21. Layer structure $\{[Ba(ba)H_2O)_2](H_2O)]_n$ (original Fig. 2 from Ref. [106]).

2.3.4. Rectangular lattice

The crystal structure of $[Cu(ca)(pyz)]_n$ (pyz = pyrazine) shows parallel sheets, which consist of square arrays of Cu^{2+} ions bridged by ca^{2-} dianions and pyrazine ligands (Fig. 19) [98]. The repeating unit Cu(ca)(pyz) develops along the *bc* plane. All the copper atoms of [Cu(ca)(pyz)] are linked by coordination bonds giving a sheet structure. The distances between the nearest neighbors Cu–ca–Cu and Cu–pyz–Cu are 7.99 and 6.98 Å, respectively. The geometry around the copper atom is a distorted elongated octahedron. The Cu–O distances are not identical (1.955(2) and 2.290(2) Å). The effect of the asymmetrical coordination is also found in the different C–O distances in the dianion (1.233(3) and 1.281(3) Å), indicating that the dianion has a *p*-quinone form structure (C–C distances: 1.369(3) and 1.537(4) Å).

2.3.5. Other layers

Dark, hydrophobic single crystals of $[Ca(Pr_2dhbq)]\cdot 2/3H_2O$ are grown in aqueous silica gel [23]. Infinite layers formed by Ca^{2+} and $[H(Pr_2dhbq)]^-$ are the main features of the crystal structure (Fig. 20). The dianion seems to have an *o*-quinone form, whereas, in one half of the anion, the bonding geometry resembles that of the corresponding anions (mean C–O distance is 1.24 Å), but in the other half the bond lengths are very similar to those observed in free 2,5-dihydroxy-benzoquinones (mean C–O distance is 1.31 Å). The remaining H atom of the anion is involved in strong intramolecular hydrogen bonding as well as in an intermolecular hydrogen bond.

The infinite layers are formed in $\{[Ba(L)(H_2O)_2]\cdot(H_2O)\}_n$ ($L = ca^{2-}$ and ba^{2-}) [106]. Four of the eight oxygen atoms around Ba^{2+} belong to the two different dianions, chelating Ba^{2+}. In this way 1D corrugated chains are formed, interlinked by two oxygen atoms of neighboring chains, thus forming layers (Fig. 21). This interconnection results from the bridging mode of the oxygen atoms. The coordination number of 8 is completed by two water molecules. The latter and a further water molecule sit between the layers. In the compounds, $\{[M(L)(H_2O)_2](H_2O)\}_n$ ($M = Ca^{2+}$, Sr^{2+}; $L = ca^{2-}$ and ba^{2-}) [107], the metal ions have an eight coordination sphere of two L anions and four water molecules. The bis-chelating dianions provide infinite chains, which are interlinked to layers by bridging two water molecules (Fig. 22). In $[Na(ca)]\cdot 3H_2O$, the anions make use of chlorine atoms to complete the six coordination of the sodium centers in the layer [108,109]. Bond lengths within the chloranilate anion are consistent with the occurrence of two independent π systems.

2.3.6. 3D structures

A 3D network of alternating ca^{2-} dianions and Pr^{3+} ions is prepared in $\{[Pr_2(ca)_3(C_2H_5OH)_6](C_2H_5OH)_2\}_n$

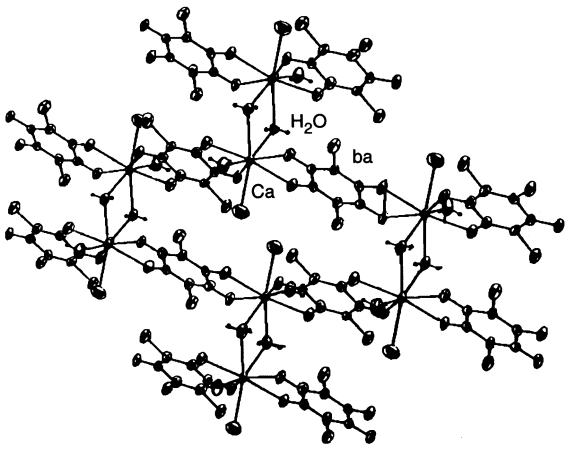

Fig. 22. Crystal structure of $\{[Ca(ba)(H_2O)_2](H_2O)\}_n$. Chains consisting of Ca^{2+} and ba^{2-} are connected to layers by common water molecules (original Fig. 2 from Ref. [22]).

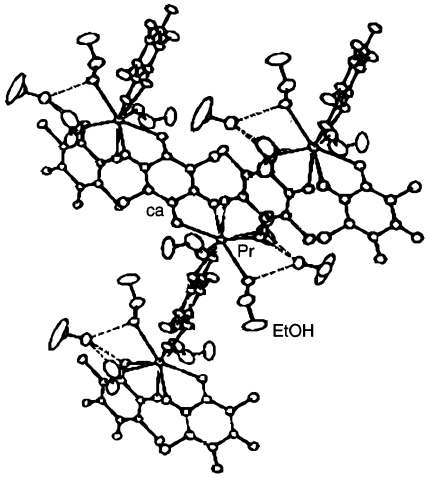

Fig. 23. Packing of the $[Pr_2(ca)_3(C_2H_5OH)_6]$ units. Hydrogen bonds are drawn as dashed line (original Fig. 1 from Ref. [110]).

(Fig. 23) [101]. The coordination sphere of Pr^{3+} consists of six oxygen atoms of the dianions and three ethanol oxygen atoms, indicating a tricapped trigonal prism. A 3D network of alternating ca^{2-} dianions and K^+ ions is prepared in $[K_2(ca)]$ [12,111]. The dianions are stacked with each other with an interplanar distance of ca. 3.42 Å along the *c*-axis.

3. Clathration and intercalation in hydrogen bond-supported layers

3.1. Host systems based on 1D polymers

Although many coordination polymers have so far been synthesized and characterized, those having 2D structures are still limited and not readily available in comparison with 1D polymers. The 2D structures are relevant for various functions such as intercalation, clathrate, and conducting and/or magnetic properties. In order to functionalize coordination compounds a rational synthesis is essential, by which tuning structures for function could be possible. The synthesis of 2D polymers greatly depends on the choice of multidentate ligand. Chloranilate and its derivatives afford one instance for this approach.

In order to synthesize 2D structures, the two step synthesis is assumed as shown in Fig. 24. According to this procedure, a 1D structure is obtained from linking ligand L, which is followed by 2D construction by another linking ligand L′. The square lattice 2D structure is obtained by using $L = ca^{2-}$ and $L' = pyz$, whose structure is mentioned in the previous section. The square array sheets of [Cu(ca)(pyz)] form the layered structure shown in Fig. 19. The nearest neighbor distance of the copper atoms is 6.98 Å, indicating closely packed layers.

On the other hand, hydrogen bonds are needed to link 1D chains to provide various 2D structures. Interestingly, the 1D motif of $\{Cu(ca)(ROH)_2\}_n$ has hydrogen bonding sites, ca–O(acceptor of H) and ROH(donor) [98]. Fig. 13 shows the layer structure with coordination bond and hydrogen bond. $[Cu(ca)(H_2O)_2]$ also affords a layer structure and the distance between the copper atoms in the different sheets is 8.45 Å. Unfortunately, the compound obtained, $[Cu(ca)(H_2O)_2]$, is thermodynamically unstable without intercalated molecules [74], which link layers tightly. Between these sheets, small molecules can be intercalated using a hydrogen-bonding interaction (Fig. 26). The first example is $\{[Cu(ca)(H_2O)_2](phz)\}_n$ where phz molecules are intercalated to form a stacked column with the distance of 3.18 Å (nearest neighbor C···C distance) [74]. The layer distance (nearest neighbor Cu···Cu distance) is 9.25 Å. Molecules of dmpyz are also introduced in between the sheets, giving a stacked column as well as phz. Interestingly, there are two types of phases (α and β) in the compound, $\{[Cu(ca)(H_2O)_2](dmpyz)\}_n$. The stacking mode of dmpyz is similar, whereas the coordination mode of dmpyz is different between α- and β-phases, leading to different colors for the compounds. This indicates the flexibility of the layer spacing. By summarizing the intercalated structures as shown in Fig. 25, the flexibility of the layer space is readily understood: the spacing between the layers, $\{[Cu(ca)(H_2O)_2]_n\}_m$, ranges from 8.45 to 11.0 Å. Here a question arises, what are factors governing intercalation of the molecules? When one takes a careful look at the structure, the following condition can be deduced. The intercalated molecule has (1) π-electronic structure to form a stacked column, and (2) hydrogen bonding sites in both the directions link the layers. They are regarded as a pillar. When condition (1) is lacking, e.g. ohphz, which has a non-

planar structure, the crystal obtained has no stacked ohphz columns. The ohphz still has hydrogen bonding capability and can hydrogen bond to the water molecules in the same chain (Fig. 9). On this basis, the pitch of the column should coincide with that of chain link, and furthermore there are several structural parameters, which are summarized in Fig. 27.

The iron(II), cobalt(II), and manganese(II) intercalation compounds $\{[M(ca)(H_2O)_2](G)\}_n$ ($M = Fe^{2+}$, Co^{2+}, Mn^{2+}, $G = H_2O$ and phenazine) have also been synthesized and characterized [73,89]. For $\{[M(ca)(H_2O)_2](H_2O)\}_n$, crystal structures consist of uncoordinated guest water molecules and 1D zigzag $[M(ca)(H_2O)_2]_k$ chains. The adjacent chains are interlinked by hydrogen bonds, thus forming layers (Fig. 28). Water molecules are intercalated between the $\{[M(ca)(H_2O)_2]_k\}_l$ layers. The intercalation mode of the water molecules is different from those in $\{[M(ca)(H_2O)_2](phz)\}_n$ ($M = Fe^{2+}$, Co^{2+}, Mn^{2+}), which are isomorphous to $\{[Cu(ca)(H_2O)_2](phz)\}_n$.

The molecular assemblies obtained here reveal three key factors that control the crystal structures. The first point is the construction of a hydrogen bond-supported 2D sheet, $\{[M(ca)(H_2O)_2]_k\}_l$, which is so flexible and amenable to intercalation of various kinds of molecules by using the hydrogen bonding interaction. The second point is that the intercalated guest molecules affect the sheet structure and dynamics of $\{[M(ca)(H_2O)_2]_k\}_l$. The third point is that the selection of the metal mediates the fine tuning of the sheet structure and the conformation of the guest molecules.

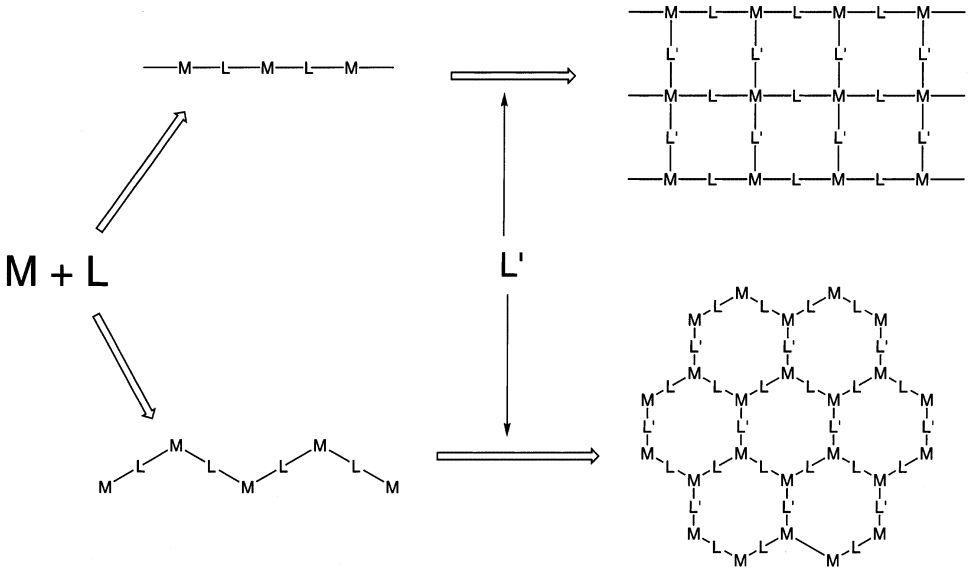

Fig. 24. Schematic illustration of construction of the 2D structure.

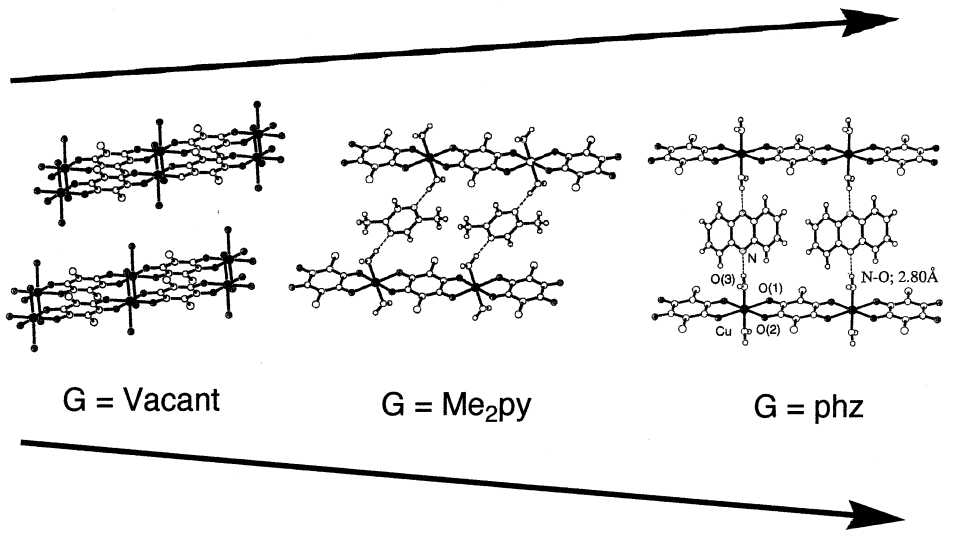

Fig. 25. Schematic illustration of the flexibility of the layer spacing.

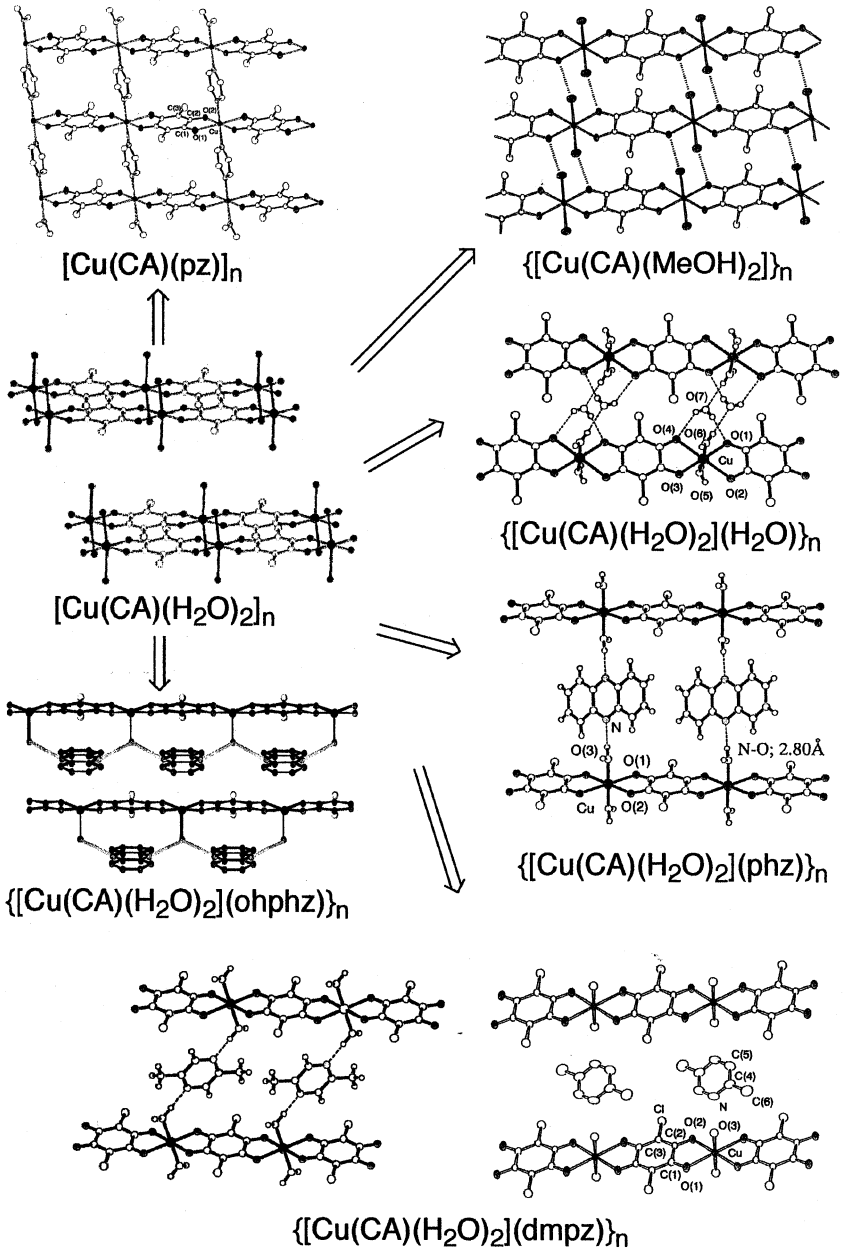

Fig. 26. Framework construction from 1D coordination polymer motifs.

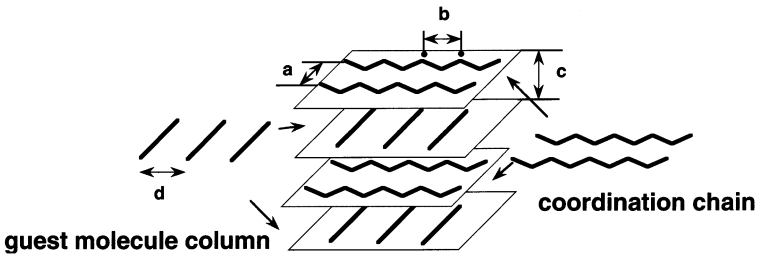

Fig. 27. Structural parameters for well-suited intercaltated structure.

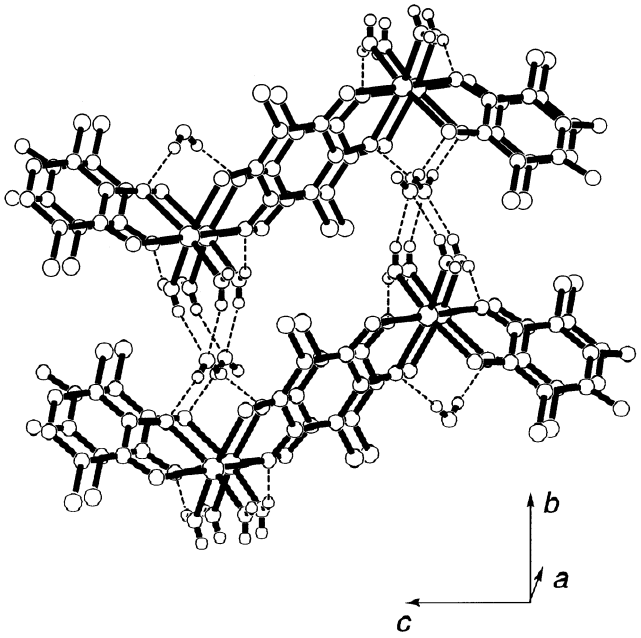

Fig. 28. Projection of $\{[Fe(ca)(H_2O)_2](H_2O)\}_n$ perpendicular to the chain (original Fig. 1-b from Ref. [73]).

3.2. Host systems based on monomer compounds

1D and 2D hydrogen bond-supported inclusion compounds which are constructed from the monomer and charged guest molecules, $\{(G)_m[M(ca)_2(H_2O)_2]\}_n$ (M^{2+} = Fe^{3+}, Cu^{2+}, Co^{2+}; G = Fc^+ [94], $Hphz^+$ [77], Hpy, H_2bpy [76], 4-pyOH_2, 3-pyOH_2 [75]) were investigated (Fig. 29). The guest cations are introduced between the $[M(ca)_2(H_2O)_2]_l^{n-}$ chains or layers. Two types of building blocks are found in $\{(G)_m[M(ca)_2(H_2O)_2]\}_n$ for constructing host structures: (1) '*trans*' type and (2) '*cis*' type monomer complexes. The inclusion mode of guest molecules in the former case is classified into two types, that is, (a) channel-included type and (b) cage-included type. For type 1-a, guest molecules are stacked to form a slipped stack column between the layers of $[M(ca)_2(H_2O)_2]_1^{2-}$, which is built from the hydrogen bonding and electrostatic interaction except for $\{(Hpy)_m[Fe(ca)_2(H_2O)_2]\}_n$. On the other hand, for type 1-b, guest molecules are trapped in the cage as a dimer. The cage is constructed by the chlorine atoms of ca^{2-} dianions of the chains, and the guest molecules are anchored by the hydrogen-bonding interaction. For type 2, the geometry around the metal ion in the building block is a distorted octahedron, but the two water molecules are coordinated to iron ion in the *cis* position relative to each other. The guest ions are included as discrete molecules between the host layers. The molecular assemblies obtained here reveal that hydrogen bond-support host assemblies, $\{[M(ca)_2(H_2O)_2]_k\}_l$, are quite flexible, capable of including various kinds of charged molecules. Both the electrostatic interaction and the hydrogen-bonding interaction are driving forces to introduce the guest molecules in these assemblies. Especially, in the case of type 1 compounds, the spacing between layers ranges from 8.91 (G = Hpy^+) to 14.57 Å ($Hphz^+$).

4. Properties

4.1. Redox properties of compounds

H_2dhbq undergoes either a one-electron oxidation or two one-electron reduction processes, yielding species with charges ranging from −4 to −1 as shown in

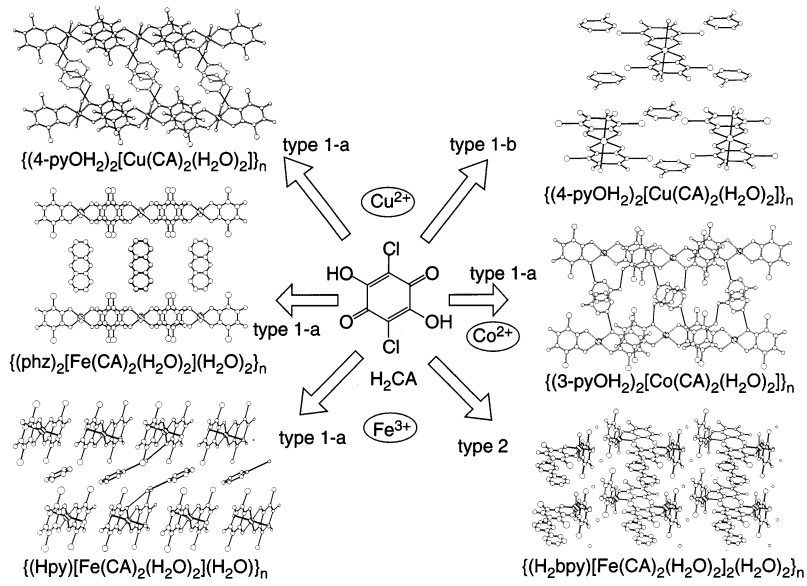

Fig. 29. Schematic illustration of hydrogen bond-supported chains and layers and their guest molecules inclusion.

Scheme 2 [91]. The species with charges -1 and -3 are radical ions. There are many transition metal compounds of the non-radical $dhbq^{2-}$ form while those of $dhbq^{n-}$ ($n = -1$, -3, and -4) are relatively sparse. Binuclear complexes of transition metal bridged by the ligand could in principle afford various valence states on transition metal and/or ligand sites, accompanied by different spin states.

Cyclic voltammograms of $M_2(cth)_2(dhbq)$ type complexes for manganese, iron and nickel show three reversible one-electron redox processes with the formation of $[M_2(cth)_2(dhbq)]^{n+}$ species ($n = 1$–4). The first process 1 in the range -1.30 to -1.42 V (vs Fc^+/Fc couple) is attributed to a ligand-centered electron transfer reaction while the other two processes 2 and 3 in the more positive region show a metal dependence, indicative of a metal-centered electron transfer. The $E_{1/2}$ potentials are listed in Table 3. The difference in $E_{1/2}$ values for processes 2 and 3 are ca. 0.2 V for manganese and nickel. The conproportionation constant (K_c) regarding the equilibrium

$$[M_2(cth)_2(dhbq)]^{4+} + [M_2(cth)_2(dhbq)]^{2+} = 2[M_2(cth)_2(dhbq)]^{3+}$$

is ca. 10^3 for Mn and Ni, while the Fe compound has well-separated redox processes ($\Delta E_{1/2} = 0.57$ V) and the value is 10^{10}. According to the peak separation it is quite difficult to isolate pure solids containing the tripositive cation of the Mn and Ni derivatives. Interestingly, the tripositive species of iron and chromium derivatives have the formulation $M^{III}(dhbq^{3-})M^{III}$, indicating that upon one-electron oxidation of the iron(II) dimer the product is not a mixed-valence species but the iron(III) dimer bridged by a dhbq radical, i.e. both the metal ions are oxidized and the ligand is reduced. A similar state is obtained in $[Cr(cth)(dhbq)]^{3+}$, which can be formulated as $Cr(III)(dhbq^3)Cr(III)$. On the other hand, the ruthenium compound $[Ru(bpy)_2(dhbq)](PF_6)_2$ in contrast to the iron and chromium complexes shows two reversible one-electron oxidation processes ($+0.36$ and 0.70 V) in acetonitrile solution, assigned to metal-based Ru(II)/Ru(III) couples [112]. The separation of 0.34 V between these couples gives conproportionation constant K_c of ca. 6×10^5. The two-fold degeneracy of the mixed valence Ru(II)/Ru(III) (class II) state, where the odd electron is associated with either metal, could be lifted by an unsymmetrical distortion involving a redistribution of electron density in dhbq. There is also a reversible one electron reduction wave at -1.05 V, which is on the predominantly ligand-centered LUMO confirmed by ESR results ($g = 2.063$).

As shown in Scheme 2, the dhbq and its derivatives can in principle bind to two metal ions as a bridge in three different oxidation states; a dianion (semiquinonate(sq), sq), a radical trianion (cat, sq), and a tetraanion (cat,cat). Rh(I) compounds, $[Rh_2(cod)_2(L)]$ ($L = dhbq^{2-}$ and ca^{2-}), are electrochemically reduced by two stepwise, reversible one-electron transfer, which

Table 3
Electrochemical potentials

Compounds	n	$E_{1/2}$ (v)							Reference	Reference electrode
	$-4/-3$	$-3/-2$	$-2/-1$	$-1/0$	$0/+1$	$+1/+2$	$+2/+3$	$+3/+4$		
$[M_2(cth)_2(dhbq)]^n$									[91]	[a]
Cr						-1.04	-0.01	–		
Mn						-1.30	0.17	0.36		
Fe						-1.31	-0.22	0.35		
Ni						-1.42	0.68	0.88		
$[Rh_2(cod)_2(dhbq)]^n$			-1.17	-0.55					[92]	[b]
$[Ru_2(bpy)_4(dhbq)]^n$						-1.05	0.36	0.70	[112]	[a]
$[Mo_2O_4(ca)Cl_4]^n$						-0.10			[119]	[c]
$[Mo_4O_{10}(dhbq)_2]^n$	-0.677	-0.208							[80]	[c]
$[Co_2(dhbq)(tdpme)_2]^n$					-1.170	-0.105			[90]	[c]
$[Co_2(ca)(tdpme)_2]^n$					-1.000	0.010			[90]	[c]
$[Co_2(ba)(tdpme)_2]^n$					-1.000	0.005			[90]	[c]
$[Co_2(ia)(tdpme)_2]^n$					-0.995	0.000			[90]	[c]
$[Co_2(na)(tdpme)_2]^n$					-0.750	0.170			[90]	[c]
$[Co_2(Me_2dhbq)(tdpme)_2]^n$					-1.250	-0.165			[90]	[c]
$[Co_2(Pr_2dhbq)(tdpme)_2]^n$					-1.245	-0.155			[90]	[c]
$[Co_2(Ph_2dhbq)(tdpme)_2]^n$					-1.175	-0.130			[90]	[c]
$[Co_2(dhbq)(tdtme)_2]^n$						-0.150			[90]	[c]
$[Co_2(dhbq)(tdxme)_2]^n$					-0.105	-1.125			[90]	[c]

[a] Fc^+/Fc in MeCN.
[b] SCE in CH_2Cl_2.
[c] SCE in MeCN.

are attributed to the (sq, sq)–(cat, sq) and to (cat, sq)–(cat, cat) couples in agreement with the ligand centered transfer processes [92]. When a tripodal phosphine ligand such as 1,1,1-tris(diphenylphosphanomethyl)ethane (tdpme) is used, the binuclear cobalt complex, $[Co_2(dhbq)(tdpme)_2](BF_4)_2$ has the (cat,cat) state of the bridging dhbq ligand [90,113]. This complex exhibits two reversible oxidation waves, the separation between these reduction waves being over 1 V corresponding to an equilibrium constant K_c for conproportionation of the neutral and the dicationic to the monocationic complex of about 10^{18}. This shows the high stability of the monocationic complex, which might be a result of delocalization of the additional electron over the whole molecule that is over both metal centers and to some extent over the bridging ligand. In the Robin and Day classification of mixed valence compounds, this complex would hence belong to class III [114–116]. The results for binuclear complexes shown here confirm that the tetraoxolene molecule has frontier orbitals with energies comparable to those of the transition-metal ions, and the nature of the reduced and oxidized species depends on the additional ligands that are present in the coordination environment.

The proximity in energy of the ligand π and metal d orbitals, in particular 3d orbitals for first transition series metal atoms, provides a new opportunity to study transition metal ion–ligand interactions. The extent of mixing of d-orbitals and ligand orbitals is evidence of the close orbital energy match and good overlap. In the case of ruthenium complexes with *o*-phenylenediamine groups, similar phenomena involving metal–ligand charge redistribution have been found. These were studied by spectroscopic, CV, and ZINDO calculations. Ruthenium complexes of 3,3′,4,4′-tetraminobiphenyl [117] and 1,2,4,5-tetraamino-3,6-diketocyclohexane [118] in the quinonediimine oxidation state show considerable d orbital mixing with dπ and LUMO and LUMO + 1 π* to much greater degrees than with 2,2′-bipyridine.

$(Bu_4N)_2[Mo_4O_{10}(dhbq)]$ exhibits two successive one-electron reduction processes which meet the criteria for diffusion-controlled reversible processes. Such processes are characteristic of ligand-based redox, rather than metal-centered processes. The EPR spectrum of the one-electron reduced species, $[Mo_4O_{10}(dhbq)]^{3-}$, exhibits a sharp single line centered at $g = 1.999$, characteristic of an unpaired electron localized on a ligand orbital. The solution and frozen sample of the two-electron reduced species, $[Mo_4O_{10}(dhbq)]^{4-}$, are EPR inactive, implying the additional electron pairs in the ligand-based electron-acceptor orbital [80]. The $[Mo_2O_4Cl_4(ca)]^{2-}$ anion is electrochemically active, displaying a one-electron reduction at -0.10 V, a process which behaves reversibly only at sweep rates greater than 2 V s^{-1} in CV and which shows characteristics associated with reduction followed by an irreversible chemical reaction [119].

4.2. Charge transfer salt compounds

Charge transfer type compounds have been synthesized using of H_2dhbq [120–125]. Bis(ethylenedioxy)tetrathiafulvalene (BEDO-TTF) reacts with H_2ca, H_2ba and H_2dhbq to give a 2:1 charge-transfer complex [126]. The crystal structure of the chloranilate complex consists of the 2D BEDO-TTF layer and the 1D stack of ca^- dianions [8]. The ionicity of the donor is estimated as $+0.5$. The electrical conductivity is 0.03 S cm^{-1} with an activation energy of 0.05 eV. The magnetic spin susceptibility is described in terms of a 1D antiferromagnet. The reaction of bis(pentamethylcyclopentadienyl)iron and H_2ca produces a 1D crystalline charge-transfer complex $[Fe(C_5Me_5)]^+$-$(Hca)^-(H_2O)$. The crystal contains water molecules that act as cohesive elements by connecting the Hca^- anions through O···H···O hydrogen bonds to form an infinite 1D supramolecular structure along the *b*-axis [127]. 4,4′-Bipyridine (bpy) and 1,2-bis(2-pyridyl)-ethylene(pde) form bifurcated hydrogen bonds with H_2ca to afford $(H_2bpy)ca$ and $(H_2pde)ca$. Their crystal structures exhibit a supramolecular synthon and link as molecular chains and zigzag tapes, respectively [128].

In the charge transfer complex prepared from OMTTF and CN_2dhbq, a trimer of the donor molecules was formed and was surrounded by the hydrogen bonded network consisted of monoanion, HCN_2dhbq [129]. The room temperature conductivity of the single crystal was 3×10^{-8} S cm^{-1}. Although the exact ionicity on each OMTTF molecule could not yet be determined, it is not erroneous to estimate the averaged charge as $+2/3$ on each donor molecule. The hydrogen bond units of the CN_2dhbq^{2-} in the charge transfer complexes are classified into four categories to characterize CN_2dhbq^{2-} as the synthon for crystal engineering [130].

4.3. Magnetic properties of compounds

The design of coupled systems with strong magnetic interactions between distant metal centers is an emerging field for inorganic chemists. The efficiency of the $C_6X_2O_4$-bridge in this respect must be mentioned. In dinuclear and polynuclear copper(II) complexes bridged by oxalato, squarate, and $C_6X_2O_4^{2-}$, the largest exchange interaction is found for the μ-oxalate complex as expected on the basis of the Cu–Cu separation, and the next largest interaction is found for the μ-$C_6X_2O_4^{2-}$ complexes [34,131–133]. The greater number of proper symmetry orbitals and their energy proximity to the copper (II) orbitals in the $C_6X_2O_4^{2-}$ dianion accounts

Table 4
Magnetic parameters of discrete complexes

Metal ion	Type	Compound	J (cm^{-1})	Reference
VO(IV)		$[VO_2(Me\text{-}phen)_2(ca)]SO_4$	15.8	[142]
		$[VO_2(phen)_2(ca)]SO_4$	8.75	[141]
		$[VO_2(Me_2\text{-}phen)_2(ca)]SO_4$	10.6	[142]
		$[VO_2(bpy)_2(ca)]SO_4$	1.18	[141]
Cu(II)	I	$[Cu_2(Me_2dien)_2(ca)](BPh_4)_2$	0.1 [b]	[135]
		$[Cu_2(Me_2dien)_2(dhbq)](BPh_4)_2$	0.1 [b]	[135]
		$[Cu_2(terpy)_2(ca)](PF_6)_2$	0.05–0.07 [b]	[136]
		$[Cu_2(terpy)_2(ca)](ClO_4)_2$	0.04–0.05 [b]	[136]
	II	$[Cu_2(dpt)_2(ca)](BPh_4)_2$	−2.0	[135]
		$[Cu_2(dpt)_2(dhbq)](BPh_4)_2$	−4.6	[135]
	III	$[Cu_2(bpy)_2(ca)](ClO_4)_2$	−14.0	[138]
		$[Cu_2(bpy)_2(ba)](ClO_4)_2$	−14.3	[138]
		$[Cu_2(phen)_2(ca)](ClO_4)_2\text{-}H_2O$	−14.0	[138]
		$[Cu_2(phen)_2(ba)](ClO_4)_2\text{-}H_2O$	−14.1	[138]
		$[Cu_2(bpy)_2(ca)](PF_6)_2\text{-}2CH_3OH$	−11.7	[138]
		$[Cu_2(bpy)_2(ba)](PF_6)_2 2H_2O$	−16.0	[138]
		$[Cu_2(phen)_2(ca)](PF_6)_2\text{-}CH_3OH$	−13.9	[138]
		$[Cu_2(phen)_2(ba)](PF_6)_2\text{-}CH_3OH$	−16.3	[138]
		$[Cu_2(tmen)_2(dhbq)](ClO_4)_2$	−10.5	[137]
		$[Cu_2(tmen)_2(ca)](ClO_4)_2$	−10.5	[137]
		$[Cu_2(tmen)_2(ba)](ClO_4)_2$	−11.3	[137]
		$[Cu_2(tmen)_2(ia)](ClO_4)_2$	−13.0	[137]
		$[Cu_2(tmen)_2(na)](ClO_4)_2$	−8.7	[137]
	VI	$[Cu_2(Me_3tacn)_2(ca)](ClO_4)_2$	−30	[139]
		$[Cu_2(Me_3tacn)_2(ca)](ClO_4)_2$	−12.3	[140]
		$[Cu_2(Me_3tacn)_2(dhbq)](ClO_4)_2$	−20	[139]
Ni(II)		$[Ni_2(tren)_2(ca)](BPh_4)_2$	−1.8	[135]
		$[Ni_2(tren)_2(dhbq)](BPh_4)_2$	−1.1	[135]
		$[Ni_2(cth)_2(dhbq)](PF_6)_2$	−2.5	[91]
Mn(II)		$[Mn_2(cth)_2(dhbq)](PF_6)_2$	−0.20	[91]
		$[Mn_2(tpa)_2(ca)](ClO_4)_2$	−0.12	[146]
		$[Mn_2(bpy)_4(ca)](ClO_4)_2$	−2.8	[147]
		$[Mn_2(phen)_4(ca)](ClO_4)_2$	−7.9	[147]
Fe(III)		$[Fe_2(H_2O)_2(ca)_3]4H_2O$	−0.95	[144]
			−0.38	[89]
		$[Fe_2(H_2O)_2(dhbq)_3]$	−2.0	[144]
		$[Fe_2(salen)_2(dhbq)_3]\cdot 1.5H_2O$	−0.92	[143]
		$[Fe_2(ca)(bpy)_4](ClO_4)_4$	−2.1	[145]
		$[Fe_2(ca)(phen)_4](ClO_4)_4$	−5.8	[145]
Gd(III)		$[Gd_2(ca)(bpy)_2]$	−1.9	[148]

[a] Calculated for Heisenberg type, $H = -2JS_1S_2$.
[b] Absolute values obtained from S–T transitions.

for the greater interaction as compared to the squarate orbitals. In spite of an M···M separation of about 7.6 Å, rather large antiferromagnetic interactions ($-J = 8$–$16\ cm^{-1}$) were found in the $C_6X_2O_4^{2-}$ bridged dinuclear and polymer copper complexes (Table 4). The J values in these compounds are significantly beyond the J_{limit} value deduced from the empirical relation proposed by Coffman and Buettner [134]

$$J_{limit}\ (cm^{-1}) = -1.35 \times 10^7 \exp(-1.80 \times R/A) \qquad (1)$$

From Eq. (1), J_{limit} is found equal to $-7.9\ cm^{-1}$ for $R = 7.59$ Å.

Four types of $C_6X_2O_4$-bridged dinuclear copper(II) complexes have been reported (Table 5). The type I compounds with a tridentate end-cap ligand show a very weak magnetic interaction [135,136]. The type II compound also has a tridentate end-cap ligand whereas the J value falls in the range from -2 to $-5\ cm^{-1}$ [135]. The geometry about each copper in types I and II is described as an intermediate between a trigonal bipyramid (tbp) and a square pyramid (sp). When a regular sp surrounding of each copper(II) ion is assumed (the basal planes are perpendicular to the plane of the bridging network), the coupling constant J becomes zero since the magnetic orbitals, x^2-y^2 type, are essentially localized in the basal planes [34,136]. Because of the actual low symmetry for copper, the metal contribution to the magnetic orbital is most purely x^2-y^2 but involves a small admixture of z^2, with a resultant delocalization on the apical site (z-direction), which allows a weak coupling. The type II compounds have larger J values than those of type I, suggesting that the coordination geometry around the copper is distorted tbp.

On the other hand, a significant antiferromagnetic interaction ($-J = 8.7$–$16.0\ cm^{-1}$) is reported for type III [137,138]. The crystal structures assume two types of coordination geometries about each copper(II): a square pyramidal or a square planar geometry with two nitrogen atoms of the end-cap ligand and two oxygen atoms of $C_6X_2O_4^{2-}$ (X = Cl and H) on the basal plane. The two basal planes in the dinuclear unit are almost coplanar. These structural features fulfill the requirements concerning the possibility of maximizing the interaction between two copper(II) ions far away from each other, that is, the HOMO of the bridge is largely delocalized on the coordinating atoms and symmetry adapted to interact with the singly occupied metal orbitals. The two frontier orbitals of b_{1g} and b_{2u} symmetries, respectively, as derived from extended Hückel calculation, are shown (Scheme 3) [135,137]. Both are largely delocalized toward the oxygen atoms with an orientation of the 2p oxygen orbitals favoring overlap with the in-phase and out-of-phase combinations of x^2-y^2 metal orbitals.

For the last class, with tridentate Me_3tacn as the end-cap ligand, unexpectedly strong antiferromagnetic interactions are reported based on the magnetic data in the limited temperature range (100–300 K). [139,140].

Table 5
Magnetic parameters of infinite complexes

Type	Ion	Compound	J (cm^{-1})[a]	Reference
1D	Cu(II)	$[Cu(dhbq)]_n$	−16.7 [b], −9.8	[30]
		$[Cu(ca)]_n$	−12.3	[33]
		$[Cu(ba)]_n$	−11.2	[33]
		$[Cu(ca)(NH_3)_2]_n$	−1.9	[33]
		$[Cu(ba)(NH_3)_2]_n$	−1.9	[33]
		$[Cu(ca)(im)_2]_n$	−1.9	[33]
		$[Cu(ca)(py)_2]_n$	−0.9	[33]
		$[Cu(ca)(anil)_2]_n$	−0.9	[33]
		$[Cu(ca)(bzim)_2]_n$	−1.0	[33]
		$[Cu(ca)(2\text{-}Meim)_2]_n$	−0.75	[33]
		$[Cu(ca)(DCMB)]_n$	−0.16	[95]
		$\{[Cu(ca)(H_2O)](ohphz)\}_n$	−10.93	[74]
	Fe(II)	$[Fe(dhbq)(H_2O)_2]_n$	−1.4	[144]
		$[Fe(ca)(H_2O)_2]_n$	−0.1	[144]
		$[Fe(ca)I]_n$	−4.0	[144]
	Mn(II)	$[Mn(ca)(bpy)_2]_n$	−0.20	[96]
		$[Mn(ca)(terpy)_2]_n$	−0.50	[105]
H-2D [c]	Cu(II)	$\{[Cu(ca)(H_2O)_2](H_2O)\}_n$	−2.04	[72]
		$\{[Cu(ca)(H_2O)_2](dmpyz)\}_n$(1a)	−1.83	[74]
		$\{[Cu(ca)(H_2O)_2](dmpyz)\}_n$(1b)	−0.39	[74]
		$\{[Cu(ca)(H_2O)_2](phz)\}_n$	−1.84	[74]
		$\{[Mn(ca)(H_2O)_2](H_2O)\}_n$	−0.74	[73]
		$\{[Mn(ca)(H_2O)_2](phz)\}_n$	−0.65	[73]
		$\{Fe(ca)(H_2O)_2](H_2O)\}_n$	+0.17	[73,89]
		$\{[Fe(ca)(H_2O)_2](phz)\}_n$	−0.65	[73]
		$\{[Co(ca)(H_2O)_2](H_2O)\}_n$	−0.45	[73]
2D	Cu(II)	$[Cu(ca)(pyz)]_n$	−2.86, −1.05 [d]	[98]
	Fe(II)	$[Fe(dhbq)(pyz)_2]_n$	−2.55	[144]
		$[Fe(ca)(pyz)_2]_n$	−0.54	[144]

[a] Calculated for Heisenberg type, $H = -2JS_1S_2$.
[b] Calculated by using an Ising Hamiltonian.
[c] Hydrogen bonding framework.
[d] zJ' value.

Two types of $C_6X_2O_4$-bridged dinuclear oxovanadium(IV) complexes have been reported ($-J = 8.8$–15.8 and $1.2\ cm^{-1}$) [141,142]. Weak antiferromagnetic interactions ($-J = 1.1 - 2.5\ cm^{-1}$) are reported for dimeric nickel(II) compounds [91,135]. Similar values of the coupling constants were reported for iron(III) complexes ($-J = 2.0$–$0.92\ cm^{-1}$) [143–145]. Two types of manganese(II) complexes have been reported ($-J =$ 0.1–$0.2\ cm^{-1}$ [91,146] and $-J = 2$–$8\ cm^{-1}$) [91,147]). A weak antiferromagnetic interaction ($-J = 1.9\ cm^{-1}$) is reported for the gadolinium(III) compound [148].

The trianionic semiquinone form of $C_6X_2O_4^{3-}$ is shown to mediate a strong magnetic interaction in dinuclear complexes of chromium(III) and iron(III). Magnetic data are consistent with a $S = 5/2$ and a $S = 9/2$ ground state for the Cr(III) and Fe(III) derivatives, respectively, as a result of a strong antiferromagnetic coupling between the metal ions and the bridging radical, that is, it can be justified with the overlap of the π^* orbital of $dhbq^{3-}$ with the t_{2g} orbitals of both Cr(III) and Fe(III) [91]. On the other hand, $\{[Co_2(C_6X_2O_4)(tdpme)_2]^{2-}$ is diamagnetic in solution and is described as a dinuclear Co(III) complex bridged by a tetraanionic $C_6X_2O_4^{4-}$ anion [90,113]. The EPR spectrum of the electrochemically singly reduced complex shows two g factors at $g_x = 2.28$ and $g_z = 2.01$ and coupling constants to the ^{57}Co nucleus ($A_x = 46$ G and $A_z = 33$ G) indicating that the additional electron is mainly localized at the metal centers.

A tetranuclear complex, $(Bu_4N)_2[Mo_4O_{10}(dhbq)_2]$ has two semiquinoid-type ligands, which stack in a parallel staggered orientation [80]. Simple electron counting requires that the ligands coordinate formally as trinegative radical anions. The most interesting feature is the short interplanar distance of 2.67 Å, between ligands allowing magnetic coupling of the radical anion ligands, which was confirmed by the observed diamagnetism.

The first structural and magnetic studies of polynuclear $Cu(C_6X_2O_4)$ compounds appeared in 1960 [27–30]. The authors noticed that two structures were possible with X = H: either a layer structure or ribbon structures. The magnetic studies showed that these compounds have ribbon structures compatible with the X-ray diffraction pattern. They proposed two alternative values for the exchange parameter in Cu(dhbq), one calculated by using an Ising Hamiltonian ($J = -16.7\ cm^{-1}$) and the other by using a Heisenberg Hamiltonian ($J = -9.8\ cm^{-1}$). EXAFS study have revealed that the compounds $Cu(C_6X_2O_4)$ and $Cu(C_6X_2O_4)L_2$, where X is Cl or Br and L a nitrogen-containing ligand such as ammonia, pyridine, imidazole, benzimidazole, 2-methyl-imidazole, or aniline, have ribbon structures [33]. The magnetic data are consistent with a chain structure, the intrachain exchange parameter J analyzed by a 1D Heisenberg-exchange model being -12.3 and $-11.2\ cm^{-1}$ for Cu(ca) and Cu(ba), respectively, and between -0.75 and $-1.9\ cm^{-1}$ for the $Cu(C_6X_2O_4)L_2$ compounds. When two L ligands are fixed per metallic center, the drastic decrease of the coupling is interpreted as a result of a reversal of the magnetic orbitals due to the rhombic distortion of the copper sites: by fixing two nitrogen containing ligands per Cu(II) ion on both sides of the $C_6X_2O_4$ ribbon plane, each Cu(II) will adopt an elongated rhombic geometry with two short Cu–N distances, two short Cu–O distances and two long Cu–O distances. This drastic modification of the site of each metallic center must induce a reversal of 90° around the O–Cu–O axis of the magnetic orbital in such a way that the new magnetic orbital points toward the nearest-neighbor nitrogen and oxygen atoms.

An analogous phenomenon has been observed for hydrogen bond supported layer compounds, $\{[Cu(ca)(H_2O)_2](G)\}_n$ which were analyzed by a 1D Heisenberg-exchange model to yield $-J = 0.4$–$2\ cm^{-1}$

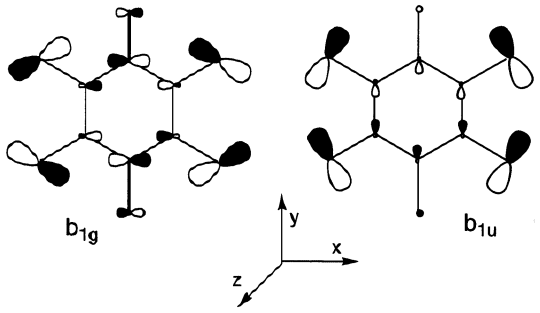

Scheme 3.

[72,74]. All the absolute values of J are smaller than the value for $[Cu(ca)]_n$ (type 1 in Scheme 4), which has a planar ribbon structure suggesting that the magnetic orbital x^2-y^2 is not parallel to the chloranilate plane but to the plane of Cu–O (H_2O) and Cu–O (chloranilate), which has short bond distances. Thus, the coordinated water molecules counter the reversal of the magnetic orbital. According to the magnitude of J, α-$\{[Cu(ca_4)(H_2O)_2](dmpyz)\}_n$ and $\{[Cu(ca)(H_2O)_2](phz)\}_n$ could be classified in the same group. Owing to the actual site symmetry D_{2h} for copper, the metallic contribution to the magnetic orbital is not purely x^2-y^2 but involves an admixture of z^2 and the mixing of the z^2 orbital of them is larger than that of β-$\{[Cu(ca)(H_2O)_2](dmpyz)\}_n$ which is demonstrated by the EPR spectra. Therefore, the spin density on the oxygen atoms of ca^{2-} in α-$\{[Cu(ca)(H_2O)_2](dmpyz)\}_n$ and $\{[Cu(ca)(H_2O)_2](phz)\}_n$ (type 2-A in Scheme 4) is larger than β-$\{[Cu(ca)(H_2O)_2](dmpyz)\}_n$ (type 2-B in Scheme 4); this accounts for the residual coupling for α-$\{[Cu(ca)(H_2O)_2](dmpyz)\}_n$ and $\{[Cu(ca)(H_2O)_2](phz)\}_n$. These features could arise from small differences in the coordination strength of the additional ligands (L) which would control the mixing of the magnetic orbital to modify the residual spin densities on the oxygen atoms of ca^{2-} and hence the magnitude of the intrachain coupling. Interestingly, these compounds exhibit the magnetic interactions tuned by hydrogen bonding. Hydrogen bonds are directional, and are thus more likely to enforce an orientation of molecules. Therefore it is easy to control the magnetic interaction by tuning the 2D structure of $[Cu(ca)(H_2O)_2]_n$, which is supported by a hydrogen bonding interaction. The J value of the five-coordinate compound, $\{[Cu(ca)(H_2O)_2](ohphz)\}_n$ ($J = -10.93$ cm^{-1}), is comparable to that of $[Cu(ca)]_n$ [74].

The EPR spectrum of a 2D lattice, $[Cu(ca)(pyz)]_n$ consists of three g values (2.304, 2.082, and 2.068) indicating that the magnetic orbital is formed mainly by the x^2-y^2 orbital. The magnetic data were analyzed using the Heisenberg linear chain theory with a mean field approximation to give $J = -2.86$ cm^{-1}, $zJ' = -1.05$ cm^{-1}. The exchange coupling constants are smaller than that for $[Cu(ca)]_n$, and comparable to that for $\{[Cu(ca)(H_2O)_2](G)\}_n$, which suggests that the magnetic orbital x^2-y^2 is no longer simply parallel to the chloranilate plane but a plane formed by Cu–N(pyz) and Cu–O vectors [98].

The magnetic behavior of the 1D compound, $[Cu(ca)(MeOH)]_n$ is different from that of $[Cu(ca)]_n$, and discrepancies indicate that the polycrystalline compound of $[Cu(ca)(MeOH)]_n$ is a new phase in copper/chloranilate systems, such as a mixed valence state or a partially reduced structure, and if so the coordinated MeOH plays an important role to control physical properties of the polymers [149].

Magnetic data obtained for the polymeric iron(II) materials are fit to an $S = 2$ Heisenberg linear-chain model with $J = -1.4$ cm^{-1} for $[Fe(dhbq)(H_2O)_2]_n$, and $J = -2.6$ cm^{-1} for $[Fe(ca)(pyz)]_n$. Corresponding values for the chloranilate-containing polymers are $J > -0.1$ cm^{-1} and $J \sim -0.5$ cm^{-1}, respectively [144]. The magnetic behavior of the mixed-valence polymer [Fe(dhbq)I] ($J = -4.0$ cm^{-1}) is dramatically different from the above polymers [132]. The $\chi_M T$ value of the straight 1D chain compound, $\{[Fe(ca)(H_2O)_2](phz)\}_n$ shows a broad maximum at around 100 K [73]. This behavior is typical of tetragonally distorted Fe(II) in which the high temperature susceptibility is dominated by a Boltzmann distribution between two terms sepa-

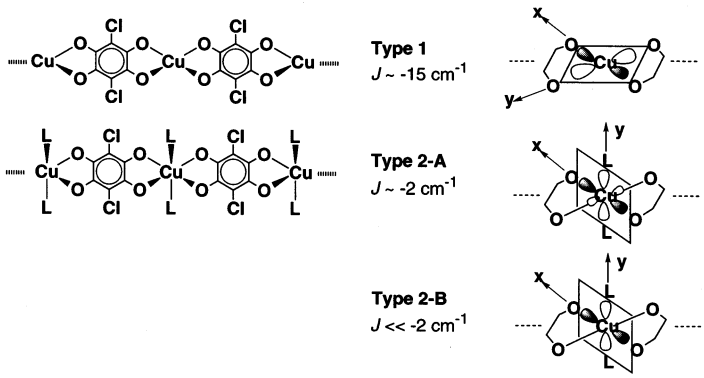

Scheme 4.

rated by about 400–700 cm^{-1}. The data were analyzed by using the infinite chain of classical spins approach derived by Fisher [133,144,150], yielding $J = -0.47$ cm^{-1}. The observed J value is the same order of magnitude as that of $\{[Mn(ca)(H_2O)_2](phz)\}_n$ [73] and can be compared with those of $[Fe(ca)(H_2O)_2]_n$ and $[Fe(dhbq)(H_2O)_2]_n$ [132,144]. These features show that the high spin ions exhibit a weak intrachain antiferromagnetic exchange interaction through chloranilate. On the other hand, the $\chi_M T$ value of the zigzag 1D chain compound $\{[Fe(ca)(H_2O)_2](H_2O)\}_n$ exhibits a minimum, but an increase (10–100 K, $\theta = 1.02$ K) and a rapid decrease (2–10 K) at lower temperature indicative of a complicated exchange interaction [73,89].

The $\chi_M T$ in the manganese and cobalt complexes decreases at lower temperature, indicative of antiferromagnetic exchange coupling. The temperature variations of the $\chi_M T$ for the manganese complexes were analyzed by using the infinite chain of classical spin approach, yield $J = -0.74$ cm^{-1} ($\{[Mn(ca)(H_2O)_2](H_2O)\}_n$) and $J = -0.65$ cm^{-1} ($\{[Mn(ca)(H_2O)_2](phz)\}_n$) [73]. The EPR signals around the $\Delta M_s = 1$ region have sharp line-widths and the $\Delta M_s = 2$ absorption [151] were observed for both cases, indicative of the existence of a spin-exchange interaction in the chains as discussed in the cases of $[Mn(bpy)(C_2O_4)]_n$ [152] and $\{[Cu(ca)(H_2O)_2](Guest)\}_n$ [74]. The J values obtained for ($\{[Mn(ca)(H_2O)_2](H_2O)\}_n$ and ($\{[Mn(ca)(H_2O)_2](phz)\}_n$ are similar to each other whereas their chain structures are different. The high-spin manganese(II) ion in an octahedral environment has a ground state, $^6A_{1g}$, which is the totally symmetric representation without first order orbital momentum. In such a case, the linking geometry in the chain may not efficiently affect the exchange interaction. However, the $|J|$ values obtained are higher than that of $[Mn(ca)(bpy)]_n$ [96] which consists of zigzag chains of manganese bridged by chloranilate and terminal bpy, whereas the Mn–Mn distance of $[Mn(ca)(bpy)]_n$ (8.142 Å) in the chain is very close to those of $\{[Mn(ca)(H_2O)_2](H_2O)\}_n$ and $[Mn(ca)(H_2O)_2](phz)\}_n$. This discrepancy could arise from a difference in the strength of the basicity between H_2O and bpy. The basicity of the terminal ligands would modify the residual spin densities on the bridging chloranilate and hence the magnitude of the intrachain coupling [33,74].

5. Conclusions

$Dhbq^{2-}$ and its derivatives are considered a unique multifunctional ligand system because they possess: (1) coordination; (2) hydrogen bonding and (3) ionic interaction sites, together with redox active π electronic structures, affording rich coordination chemistry. From the spatial structural point of view, various types of metal complexes, most of which are listed in this article, have been synthesized. By taking advantage of the ligand multifunctionality, one could create a wide variety of assembled structures, whose motifs range from mononuclear, polynuclear to infinite forms. In particular, layered frameworks are rationally realized with the aid of self-assembly processes. Building layered structures from this ligand system would open up a new dimension to coordination chemistry as well as metal oxides and phosphates [153]. From the electronic structural point of view, the polyoxocarbon molecules have frontier orbitals with energies comparable to those of the transition metal ions and the nature of the reduced and oxidized species depends on the metal ions and the coordination environment. The proximity in energy of the ligand π and metal d orbitals, in particular 3d orbitals for first transition series metal atoms, provides a new aspect for coupling the anion radical and transition metal ion d orbitals, in the various redox isomers. It is useful to estimate the extent of the mixing of d-orbitals and the ligand orbitals since this is the evidence of the close orbital energy match and the good overlap. The recent ZINDO calculations of ruthenium complexes with 3,3′,4,4′-tetraminobiphenyl [117] and 1,2,4,5-tetraamino-3,6-diketocyclohexane [118] afford a hint for a quantitative interpretation of this sort of system.

The redox isomerism based on the ligand and the transition metal sites provide useful synthons to create an assembled system, which would provide cooperative charge and spin properties. Self-assembly processes offer a particularly attractive approach for preparing such entities. Especially, the generation of arrays by metal complexes and guest molecules is interesting in this respect, as the presence of guest molecules may endow the resulting organic–inorganic hybrid architecture with novel redox, optical, magnetic, and other properties enhanced by host–guest interaction. A still intriguing challenge is a doping for Fe(II)/dhbq complexes where a mixed valence iron coordination polymer with dhbq was obtained by solid-state I_2 oxidation [132,144]. The basis of this chemistry is the formation of layer compounds by using redox active transition metals such as iron and dhbq derivatives. Structural chemistry now, appears to have matured. In this context, new functional chemistry for metal complexes of dhbq and its derivatives have just begun and will provide us with fruitful materials.

Acknowledgements

The ministry of Education for Science, Sports and Culture is acknowledged for their financial support.

References

[1] R. West, Oxocarbons, Academic Press, New York, 1980.
[2] R. West, D.L. Powell, J. Am. Chem. Soc. 85 (1963) 2577.
[3] E.K. Andersen, Acta Crystallogr. 22 (1967) 191.
[4] E.K. Andersen, Acta Crystallogr. 22 (1967) 188.
[5] E.K. Andersen, Acta Crystallogr. 22 (1967) 196.
[6] E.K. Andersen, Acta Crystallogr. 22 (1967) 201.
[7] E.K. Andersen, Acta Crystallogr. 22 (1967) 204.
[8] S. Horiuchi, H. Yamochi, G. Saito, K. Matsumoto, Synth. Met. 86 (1997) 1809.
[9] E.K. Andersen, I.G.K. Andersen, Acta Crystallogr. B 31 (1975) 384.
[10] E.K. Andersen, I.G.K. Andersen, Acta Crystallogr. B 31 (1975) 379.
[11] Z.G. Aliev, S.I. Kondrat'ev, L.O. Atovmyan, M.L. Khidekel, V.V. Karpov, Izv. Akad. Nauk. SSSR Ser. Khim. (1981) 487.
[12] V.S. Kulpe, J. Prakt. Chem. 316 (1974) 353.
[13] D. Semmingsen, Acta Chem. Scand. B 31 (1977) 11.
[14] M. Soriano-Garcia, R.A. Toscano, E. Flores-Valverde, F. Montoya-Vega, I. Lopez-Celis, Acta Crystallogr. C 42 (1986) 1576.
[15] C. Robl, Z. Kristallogr. 184 (1988) 289.
[16] J.A. Kanters, A. Schouten, A.J.M. Duisenberg, T. Glowiak, Z. Malarski, L. Sobczyk, E. Grech, Acta. Crystallogr. C 47 (1991) 2148.
[17] J.M. Williams, S.W. Peterson, Acta Crystallogr. A 25 (1969) S113.
[18] M. Munakata, L.P. Wu, T. Kuroda-Sowa, M. Yamamoto, M. Maekawa, K. Moriwaki, Inorg. Chim. Acta 268 (1998) 317.
[19] H.P. Klug, Acta Crystallogr. 19 (1965) 983.
[20] C. Robl, Mat. Res. Bull. 22 (1987) 1395.
[21] C. Robl, A. Weiss, Z. Anorg. Allg. Chem. 546 (1987) 152.
[22] C. Robl, W.F. Kuhs, J. Solid State Chem. 74 (1988) 21.
[23] C. Robl, G.M. Sheldrick, Z. Naturforsch. 43b (1988) 733.
[24] C. Robl, G.M. Scheldrick, Z. Kristallogr. 184 (1988) 295.
[25] C. Robl, Z. Kristallogr. 180 (1987) 249.
[26] S. Kanda, Y. Saito, Bull. Chem. Soc. Jpn. 30 (1957) 192.
[27] S. Kanda, Bull. Chem. Soc. Jpn., Pure Chem. Sect. 81 (1960) 1347.
[28] S. Kanda, Bull. Chem. Soc. Jpn. Pure Chem. Sect. 83 (1962) 282.
[29] S. Kanda, Bull. Chem. Soc. Jpn. Ind. Chem. Sect. 66 (1963) 641.
[30] H. Kobayashi, T. Haseda, E. Kanda, J. Phys. Soc. Jpn. 18 (1963) 349.
[31] H. Kobayashi, T. Haseda, E. Kanda, S. Kanda, J. Phys. Soc. Jpn. 18 (1963) 349.
[32] R. Sartene, F.H. Boutron, Mol. Phys. 18 (1970) 825.
[33] M. Verdaguer, A. Michalowicz, J.J. Girerd, N. Alberding, O. Kahn, Inorg. Chem. 19 (1980) 3271.
[34] O. Kahn, Angew. Chem. Int. Ed. Engl 24 (1985) 834.
[35] T.R. Rao, P. Lingaiah, L. Sirdeshmukh, S. Mehdi, J. Indian Chem. Soc. 66 (1989) 826.
[36] T.R. Rao, P.R. Rao, P. Lingaiah, L.S. Deshmukh, J. Indian. Chem. Soc. 68 (1991) 458.
[37] J.E. Earley, O. Olubuyide, K. Lu, J. Indian Chem. Soc. 69 (1992) 481.
[38] D. Prakash, R.N. singh, R.L. Verma, O.P. Gupta, J. Indian Chem. Soc. 68 (1991) 518.
[39] B.S. Garg, R. Dixit, N. Kiran, Ann. Chim. 81 (1991) 155.
[40] S. Sudoh, T. Miyanaga, S. Ohta, Y. Nagao, S. Katagiri, Chem. Lett. (1990) 2243.
[41] S. Sudoh, T. Miyanaga, Chem. Lett. (1993) 2171.
[42] S. Sudoh, T. Miyanaga, Jpn. J. Appl. Phys. S32-2 (1993) 821.
[43] T. Miyanaga, S. Sudoh, Physica B 208&209 (1995) 575.
[44] S. Sudoh, R. Miyamoto, K. Kudoh, Kidorui 28 (1996) 256.
[45] S. Sudoh, R. Miyamoto, M. Nobunari, M. Hiroki, K. Kudo, Kidorui 26 (1995) 92.
[46] H. Miyoshi, M. Matsumoto, S. Kanda, J. Colloid Interface Sci. 193 (1997) 26.
[47] J. Kuyper, Inorg. Chem. 18 (1979) 1484.
[48] K. Ueno, F. Sagara, K. Higashi, K. Yakata, I. Yoshida, D. Ishii, Anal. Chim. Acta 261 (1992) 241.
[49] A.M. Dona, J.F. Verchere, Analyst 116 (1991) 533.
[50] I.J.E. Barney, D.D. Rosebrook, Anal. Chim. Acta 58 (1972) 131.
[51] G. Beswick, R.M. Johnson, Talanta 17 (1970) 709.
[52] A.M. Talati, V.N. Mistry, J. Indian Chem. Soc. 50 (1973) 225.
[53] J.M. Poirier, J.F. Verchere, Talanta 26 (1979) 349.
[54] J.F. Verchere, J. Chem. Res. Synop. (1978) 178.
[55] J.F. Verchere, J.M. Poirier, J. Inorg. Nucl. Chem. 42 (1980) 1514.
[56] J.M. Poirier, J.F. Verchere, J. Chem. Res. Synop. (1980) 80.
[57] H. Huber, H. Raber, K. Dvorak, K. Kalcher, Mikrochim 1 (1982) 155.
[58] O.I. Villegas, O. Baudino, V.A. Cortinez, C.B. Marone, Ann. Asoc. Quim. Argent. 71 (1983) 113.
[59] G. Bianchi, C.B. Marone, J. Inorg. Nucl. Chem. 43 (1981) 2985.
[60] J. Toei, Analyst 112 (1987) 1067.
[61] M. Mallea, J. Raba, S. Quintar, G. Narda, V. Cortinez, J. Pedregosa, J. Mater. Sci. Lett 8 (1989) 397.
[62] B.S. Garg, R. Dixit, N. Kiran, J.L. Sharma, Bull. Chem. Chim. Fr. (1989) 168.
[63] M.I. Karayannis, P.G. Veltsistas, Analyst 115 (1990) 741.
[64] K. Yakata, F. Sagara, I. Yoshida, K. Ueno, Anal. Sci. 6 (1990) 711.
[65] M. Kamaya, Y. Hamada, S. Yazaki, K. Nagashima, E. Ishii, Anal. Chim. Acta 264 (1992) 131.
[66] F. Sagara, T. Tsuji, I. Yoshida, D. Ishii, K. Ueno, Anal. Chim. Acta 270 (1992) 217.
[67] R.A. Holwerda, J.S. Kim, T.W. Robison, R.A. Bartsch, B.P. Czech, J. Organomet. Chem. 443 (1993) 123.
[68] A. Yamada, K. Hodouchi, H. Matsubara, Denki Kagaku oyobi Kogyo Butsuri Kagaku 61 (1993) 834.
[69] J. Zarebski, G. Henze, Chem. Anal. 43 (1998) 15.
[70] J.L. Guil, M.E. Torija, J.J. Gimenez, I. Rodriguez-Garcia, A. Gimenez, J. Agric. Food. Chem. 44 (1996) 1821.
[71] S. Kitagawa, M. Kondo, Bull. Chem. Soc. Jpn. 71 (1998) 1739.
[72] S. Kawata, S. Kitagawa, M. Kondo, M. Katada, Synth. Metals 71 (1995) 1917.
[73] S. Kawata, S. Kitagawa, H. Kumagai, T. Ishiyama, K. Honda, H. Tobita, K. Adachi, M. Katada, Chem. Mater. 10 (1998) 3902.
[74] S. Kawata, S. Kitagawa, H. Kumagai, C. Kudo, H. Kamesaki, T. Ishiyama, R. Suzuki, M. Kondo, M. Katada, Inorg. Chem. 35 (1996) 4449.
[75] S. Kawata, S. Kitagawa, K. Adachi, H. Kumagai, K. Iijima1, J. Chem. Soc. Dalton Trans. (2000) 2409.
[76] M.K. Kabir, N. Miyazaki, S. Kawata, K. Adachi, H. Kumagai, K. Inoue, S. Kitagawa, K. Iijima, M. Katada, Coord. Chem. Rev. 198 (2000) 157.
[77] M.K. Kabir, S. Kawata, K. Adachi, H. Tobita, N. Miyazaki, H. Kumagai, M. Katada, S. Kitagawa, Mol. Cryst. Liq. Cryst. 341 (2000) 491.
[78] R. Robson, J.C.S. Dalton Trans. (2000) 3735.
[79] S. Liu, S.N. Shaikh, J. Zubieta, Inorg. Chem. 27 (1988) 3064.
[80] S. Liu, S.N. Shaikh, J. Zubieta, Inorg. Chem. 28 (1989) 723.
[81] O.N. Krasochka, V.A. Avilov, L.O. Otovmyan, Zh. Struckt. Khim. 15 (1974) 1140.
[82] W.-Y. Jeong, R.A. Holwerda, Inorg. Chem. 27 (1988) 4316.
[83] W.-Y. Jeong, R.A. Holwerda, Inorg. Chem. 27 (1988) 2571.

[84] W.-Y. Jeong, R.A. Holwerda, J. Organomet. Chem. 372 (1989) 453.
[85] W.-Y. Jeong, R.A. Holwerda, Inorg. Chem. 28 (1989) 2674.
[86] R.F. Johnston, P.K.S. Gupta, M.B. Ossain, R.v.d. Helm, W.-Y. Jeong, R.A. Holwerda, Acta Crystallogr. C 46 (1990) 1796.
[87] R.F. Johnston, D.G.v.d. Veer, R.A. Holwerda, J. Cryst. Spectrosc. Res. 22 (1992) 755.
[88] A.J. Bessire, B.R. Whittlesey, R.A. Holwerda, Inorg. Chem. 34 (1995) 622.
[89] B.F. Abrahams, K.D. Lu, B. Moubaraki, K.S. Murray, R. Robson, J. Chem. Soc. Dalton Trans. (2000) 1793.
[90] K. Heinze, G. Huttner, L. Zsolnai, A. Jacobi, P. Schober, Chem. Eur. J. 3 (1997) 732.
[91] A. Dei, D. Gatteschi, L. Pardi, U. Russo, Inorg. Chem. 30 (1991) 2589.
[92] M.A. Calvo, A.M.M. Lanfredi, L.A. Oro, M.T. Pinillos, C. Tejel, A. Tiripicchio, F. Ugozzoli, Inorg. Chem. 32 (1993) 1147.
[93] S. Liu, S.N. Shaikh, J. Zubieta, J. Chem. Soc. Chem. Commun. (1988) 1017.
[94] S. Kawata, H. Kumagai, S. Kitagawa, K. Honda, M. Enomoto, M. Katada, Mol. Cryst. Liq. Cryst. 286 (1996) 51.
[95] S. Decurtins, H.W. Schmalle, L. Zheng, J. Ensling, Inorg. Chim. Acta 244 (1996) 165.
[96] L. Zheng, H.W. Schmalle, R. Huber, S. Decurtins, Polyhedron 15 (1996) 4399.
[97] W. Frenzer, R. Wartchow, H. Bode, Z. Kristallogr. 212 (1997) 237.
[98] S. Kawata, S. Kitagawa, M. Kondo, I. Furuchi, M. Munakata, Angew. Chem. Int. Ed. Engl. 33 (1994) 1759.
[99] C. Robl, A. Weiss, Z. Naturforsch. 41b (1986) 1337.
[100] C. Robl, Z. Naturforsch. 42b (1987) 972.
[101] C. Robl, W.F. Kuhs, J. Solid State Chem. 79 (1989) 46.
[102] A. Weiss, E. Riegler, C. Robl, Z. Naturforsch. 41b (1986) 1501.
[103] B.F. Abrahams, J. Coleiro, B.F. Hoskins, R. Robson, J. Chem. Soc., Chem. Commun. (1996) 603.
[104] C. Robl, Mater. Res. Bull. 22 (1987) 1483.
[105] M.K. Kabir, M. Kawahara, H. Kumagai, K. Adachi, S. Kawata, T. Ishii, S. Kitagawa, Polyhedron, in press.
[106] C. Robl, A. Weiss, Z. Naturforsch. 41 (1986) 1495.
[107] C. Robl, A. Weiss, Mater. Res. Bull. 22 (1987) 497.
[108] R. Benchekroun, J.-M. Savariault, Acta. Crystallogr. C 51 (1995) 186.
[109] C. Papadimitriou, P. Veltsistas, J. Marek, J. Novosad, A.M.Z. Slawin, J.D. Woollins, Inorg. Chem. Commun. 1998 (1998) 418.
[110] P.E. Riley, S.F. Haddad, K.N. Raymond, Inorg. Chem. 22 (1983) 3090.
[111] H. Bock, S. Nick, C. Näther, J.W. Bats, Z. Naturforsch. 49b (1994) 1021.
[112] M. Ward, Inorg. Chem. 35 (1996) 1712.
[113] K. Heinze, G. Huttner, O. Walter, Eur. J. Inorg. Chem. (1999) 593.
[114] M.B. Robin, P. Day, Adv. Inorg. Chem. Radiochem. 10 (1967) 247.
[115] D.B. Brown, ed. Mixed Valence Compounds, Reidel Publ., Doedrecht, Holland, 1980.
[116] C. Creutz, Prog. Inorg. Chem. 30 (1983) 1.
[117] R.A. Metcalfe, L.C.G. Vasconcellos, H. Mirza, D.W. Franco, A.B.P. Lever, J. Chem. Soc. Dalton Trans. (1999) 2653.
[118] H. Masui, A.L. Freda, M.C. Zerner, A.B.P. Lever, Inorg. Chem. 39 (2000) 141.
[119] S.N. Shaikh, J. Zubieta, Inorg. Chim. Acta 146 (1988) 149.
[120] V. Rodriguez, J.M. Gutierres-Zorrilla, P. Vitoria, A. Luque, P. Roman, M. Martinez-Ripoll, Inorg. Chim. Acta 290 (1999) 57.
[121] M.B. Zaman, Y. Morita, J. Toyoda, H. Yamochi, G. Saito, N. Yoneyama, T. Enoki, K. Nakasuji, (1997) Chem. Lett., 729.
[122] M.B. Zaman, M. Tomura, Y. Yamashita, Org. Lett. 2 (2000) 273.
[123] H. Ishida, S. Kashino, Acta Crystallogr. C 55 (1999) 1149.
[124] H. Ishida, S. Kashino, Acta Crystallogr. C 55 (1999) 1923.
[125] H. Ishida, S. Kashino, Acta Crystallogr. C 55 (1999) 1714.
[126] S. Horiuchi, H. Yamochi, G. Saito, K. Sakaguchi, M. Kusunoki, J. Am. Chem. Soc. 118 (1996) 8604.
[127] M.B. Zaman, M. Tomura, Y. Yamashita, M. Sayaduzzaman, A.M.S. Chowdhury, Cryst. Eng. Commun. (1999) 9.
[128] M.B. Zaman, M. Tomura, Y. Yamashita, Chem. Commun. (1999) 999.
[129] M.B. Zaman, J. Toyoda, Y. Morita, S. Nakamura, H. Yamochi, G. Saito, K. Nakasuji, Synth. Met. 102 (1999) 1691.
[130] H. Yamochi, S. Nakamura, G. Saito, M.B. Zaman, J. Toyoda, Y. Morita, K. Nakasuji, Y. Yamashita, Synth. Met. 102 (1999) 1729.
[131] T.R. Felthouse, D. Hendrickson, Inorg. Chem. 9 (1978) 2636.
[132] J.T. Wrobleski, D.B. Brown, Inorg. Chem. 18 (1979) 2738.
[133] O. Kahn, Molecular Magnetism, VCH, New York, 1993.
[134] R.E. Coffman, G.R. Buettner, J. Phys. Chem. 83 (1979) 2387.
[135] C.G. Pierpont, L.C. Francesconi, D.N. Hendrickson, Inorg. Chem. 16 (1977) 2367.
[136] J.V. Folgado, R. Ibáñez, E. Coronado, D. Beltrán, J.M. Saavariault, J. Galy, Inorg. Chem. 27 (1988) 19.
[137] F. Tinti, M. Verdaguer, O. Kahn, J.-M. Savariault, Inorg. Chem. 26 (1987) 2380.
[138] C. Fujii, M. Mitsumi, M. Kodera, K. Motoda, M. Ohba, N. Matsumoto, H. Okawa, Polyhedron 13 (1994) 933.
[139] P. Chaudhuri, K. Oder, J. Chem. Soc. Dalton Trans. (1990) 1597.
[140] S. Gallert, T. Weyhermuller, K. Wieghardt, P. Chaudhuri, Inorg. Chim. Acta 274 (1998) 111.
[141] C.-W. Yan, Y.-T. Li, D.-Z. Liao, Synth. React. Inorg. Met.-Org. Chem. 27 (1997) 1047.
[142] Y.-T. Li, C.-W. Yan, D.-Z. Liao, Chin. J. Chem. 16 (1998) 118.
[143] F. Lloret, M. Julve, J. Faus, X. Solans, Y. Journaux, I. Morgenstern-Badarau, Inorg. Chem. 29 (1990) 2232.
[144] J.T. Wrobleski, D.B. Brown, Inorg. Chem. 18 (1979) 498.
[145] Y.-T. Li, C.-W. Yan, Y.-J. Zheng, D.-Z. Liao, Polyhedron 17 (1998) 1423.
[146] D.F. Xiang, C.Y. Duan, X.S. Tan, Y.J. Liu, W.X. Tang, Polyhedron 17 (1998) 2647.
[147] Y.-T. Li, C.-W. Yan, D.-Z. Liao, Pol. J. Chem. 71 (1997) 1511.
[148] C. Deng, Z. Jiang, D. Liao, S. Yan, G. Wang, Zhongguo Xitu Xuebao 11 (1993) 78.
[149] S. Kawata, S. Kitagawa, I. Furuchi, C. Kudo, H. Kamesaki, M. Kondo, M. Katada, M. Munakata, Mol. Cryst. Liq. Cryst. 274 (1995) 179.
[150] M.E. Fisher, Am. J. Phys. 32 (1964) 343.
[151] A. Bencini, D. Gatteschi, EPR of Exchange Coupled Systems, Springer, Berlin, 1990.
[152] D. Deguenon, G. Bernardinelli, J.-P. Tuchagues, P. Castan, Inorg. Chem. 29 (1990) 3031.
[153] T.E. Mallouk, J.A. Gavin, Acc. Chem. Res. 31 (1998) 209.
[154] H. Burzlaff, J. Lange, R. Spengler, Acta Crystallogr. C 51 (1995) 190.
[155] A. Bram, G. Bruederl, H. Burzlaff, J. Lange, W. Rothammel, R. Spengler, Acta Crystallogr. C 50 (1994) 178.
[156] R. Spengler, J. Lange, H. Zimmermann, H. Burzlaff, Acta Crystallogr. B 51 (1995) 174.
[157] B.F. Abrahams, B.F. Hoskins, R. Robson, Acta Crystallogr. C 52 (1996) 2766.
[158] S. Decurtins, H.W. Schmalle, P. Schneuwly, L. Zheng, Acta Crystallogr. C 52 (1996) 561.

[159] L.-M. Zheng, H.W. Schmalle, S. Ferlay, S. Decurtins, Acta Crystallogr. C 54 (1998) 1578.
[160] A. Elduque, Y. Carcés, L.A. Oro, M.T. Pinillos, A. Tiripicchio, F. Ugozzoli, J. Chem. Soc. Dalton Trans. (1996) 2155.
[161] J.M. Casas, L.R. Falvello, J. Fornies, G. Mansilla, A. Martin, Polyhedron 18 (1999) 403.
[162] P. Veltsistas, C. Papadimitriou, Y. Arabatzis, A.M.Z. Slawin, J.D. Woollins, Phosphorus, Sulfur Silicon Relat. Elem. 124&125 (1997) 407.
[163] M.K. Kabir, S. Kawata, K. Adachi, H. Kumagai, S. Kitagawa, Mol. Cryst. Liq. Cryst. 342 (2000) 211.
[164] S. Cueto, H.-P. Straumann, P. Rys, W. Petter, V. Gramlich, F. Rys, Acta Crystallogr. C 48 (1992) 458.